A fluorescence microscopy based immunoassay for the specific detection and quantitation of alpha-synuclein aggregates

Inaugural dissertation

for the attainment of the title of doctor
in the Faculty of Mathematics and Natural Sciences
at the Heinrich Heine University Düsseldorf

presented by

Steffen Hübinger
from Düsseldorf

Düsseldorf, 01 2015

from the Institut für Physikalische Biologie
at the Heinrich Heine University Düsseldorf

Published by permission of the
Faculty of Mathematics and Natural Sciences at
Heinrich Heine University Düsseldorf

Supervisor: Prof. Dr. Dieter Willbold
Co-supervisor: Prof. Dr. Alfons Schnitzler

Date of the oral examination: February 3rd 2015

Table of contents

1 Introduction 5
1.1 Synucleinopathies 5
1.1.1 Parkinson's disease 5
1.1.2 Dementia with Lewy bodies 6
1.1.3 Multiple-system atrophy 6
1.2 α-synuclein 7
1.2.1 Fibrillar structure of α-synuclein 8
1.2.2 Assessing conformational change during aggregation 9
1.2.3 Toxicity of α-synuclein 10
1.3 α-synuclein as a biomarker for synucleinopathies 10
1.4 Surface-Fluorescence Intensity Distribution Analysis (sFIDA) 11
1.5 Aim of the thesis 13
2 Materials and Methods 14
2.1 Materials and Chemicals 14
2.1.1 Buffers and Solutions 14
2.1.2 Antibodies 15
2.2 Recombinant expression of α-synuclein 15
2.2.1 Expression protocol 15
2.3 Purification of recombinant α-synuclein 16
2.3.1 Cell lysis 16
2.3.2 Thermal denaturation 16
2.3.3 Ammonium sulphate precipitation 16
2.3.4 Ion exchange chromatography (IEC) 17
2.3.5 Size exclusion chromatography (SEC) 17
2.4 Determination of protein concentration by absorption spectroscopy 17

2.5 Determination of concentration of aggregated α-synuclein by absorption spectroscopy 18

2.6 Gel electrophoresis and protein staining 18

2.6.1 Denaturing gel electrophoresis (SDS-PAGE) 18

2.6.2 Coomassie Brilliant Blue protein staining 19

2.6.3 Western blotting and immunostaining 19

2.7 Aggregation of α-synuclein 20

2.8 Biophysical characterisation of α-synuclein aggregate formation 20

2.8.1 Circular dichroism (CD) spectroscopy 21

2.8.2 Thioflavin T (ThT) fluorescence assay 21

2.8.3 Atomic force microscopy (AFM) 22

2.9 Fluorescent labelling of antibodies 22

2.9.1 Labelling of antibodies with Alexa Fluor 488 22

2.9.2 Labelling of antibodies with Alexa Fluor 633 23

2.9.3 Surface Plasmon Resonance (SPR) measurements of labelled antibodies 23

2.10 Surface-based Fluorescence Intensity Distribution Analysis (sFIDA) 24

2.10.1 Preparation of the surface 25

2.10.2 Measurement by Total Internal Reflection Fluorescence Microscopy (TIRFM) 28

2.10.3 Measurement by Confocal Laser Scanning Microscopy (CLSM) 30

2.11 Evaluation of sFIDA measurements 32

2.11.1 Colocalisation of images 32

2.11.2 Outlier test 33

2.11.3 Cutoff determination 34

2.11.4 Evaluation of TIRFM measurements 35

2.11.5 Evaluation of CLSM measurements 35

3 Results 37

3.1 Production of α-synuclein 37

3.1.1 Expression of α-synuclein in *E. coli* 37

3.1.2 Purification of α-synuclein 38
3.2 Fibrillation of α-synuclein 41
3.2.1 Change in secondary structure during fibrillation 41
3.2.2 Change in ThT fluorescence during fibrillation 44
3.2.3 Visualisation of aggregates by AFM 44
3.2.4 Suitability of different fibrils for sFIDA 47
3.3 Storage of fibrils 49
3.3.1 Change in fibril concentration depending on storage conditions 50
3.3.2 AFM measurements of fibrils after storage 50
3.3.3 sFIDA measurements of fibrils after storage 52
3.4 Preparation of fluorescently labelled antibodies 53
3.4.1 SPR measurements of labelled antibodies 53
3.5 sFIDA establishment 56
3.5.1 Comparing different antibody combinations 56
3.5.2 Validation of sFIDA measurements in buffer and CSF 58
3.6 Analysis of CSF from patients with synucleinopathies by sFIDA 60
3.6.1 sFIDA measurements of MSA samples 60
3.6.2 sFIDA measurements of PD samples 61
4 Discussion 63
4.1 Expression and purification of α-synuclein in high yield and purity 63
4.2 Fibrillation of α-synuclein and comparison of different buffer systems 64
4.2.1 Change in secondary structure occurs fastest in NaP_i/SDS buffer 65
4.2.2 Formation of ThT-positive α-synuclein aggregates occurs within 24 h in all buffers 65
4.2.3 Fibrils obtained in all buffers show similar morphology in AFM 66
4.2.4 Fibrils formed in NaP_i/SDS are most suitable for sFIDA 66
4.2.5 Conclusion: NaP_i/SDS buffer assures fast fibril formation and high signal intensity in sFIDA 66
4.3 Storage of α-synuclein fibrils 67

4.3.1 Loss of α-synuclein fibrils is lowest if fibrils are stored in buffer at -80 °C 67

4.3.2 Fibril morphology is not affected by storage as analysed by AFM 68

4.3.3 sFIDA reveals little difference between storing methods if equal amounts of aggregates are applied 68

4.3.4 Conclusion: Storing fibrils in buffer at -80 °C is the preferable method, but the fibril concentration needs to be reassessed before further use 68

4.4 SPR measurements indicate no loss of function of antibodies through labelling 69

4.5 Establishing sFIDA with recombinant aggregates 70

4.5.1 Choice of capture antibody as well as colocalisation of images are critical for sFIDA 70

4.5.2 sFIDA enables detection of α-synuclein aggregates in CSF 71

4.5.3 sFIDA adaption to clinical samples 72

5 Summary 75

6 Zusammenfassung 76

7 List of Figures and Tables 78

7.1 Figures 78

7.2 Tables 79

8 Literature 80

Eidesstattliche Erklärung 88

Danksagung 89

1 Introduction

1.1 Synucleinopathies

Synucleinopathies are a group of neurodegenerative diseases characterised by the abnormal accumulation of α-synuclein in aggregates, typically occurring in neurons and glial cells. The three most prevalent diseases are Parkinson's Disease (PD), Multiple-system atrophy (MSA) and dementia with Lewy bodies (DLB) (McCann et al. 2014). They are defined by a chronic and progressive decline in motor, cognitive, behavioural and autonomic functions caused by loss of neuronal cells. The symptoms often overlap, complicating differential diagnosis. Therefore the term synucleinopathies has little value for the clinician in the context of diagnosis, despite the similarities in the biochemical background of the diseases (Marti et al. 2003). Clinical symptoms cover a range of neuronal deficiencies, including motor skill impairment, dementia and sleep disorders, but misfolded α-synuclein inclusions are the common, defining feature of PD, MSA and DLB (Spillantini et al. 1998).

1.1.1 Parkinson's disease

PD is the most common of the synucleinopathies, and following Alzheimer's disease the second most common age-related neurodegenerative disorder (Goldmann et al. 2007). It affects primarily motor skills of patients and is characterised by four cardinal symptoms: tremor, rigor, bradykinesia and postural instability. The cause for the motor symptoms is the mainly the death of dopaminergic neurons in the subsantia nigra, a region in the midbrain involved in inhibiting involuntary movement. However, many patients also suffer from cognitive impairment or sleep disorders (Jankovic 2008).

PD is considered to be an idiopathic disease, although some genetic risk factors have been found. Mutation in the genes coding of α-synuclein (SNCA), ubiquitin C-terminal hydrolase like 1 (UCH-L1) and parkin (PRKN), as well as LRRK2, DJ-1 and PINK 1 have been found to be correlated to PD in a small number of patients (Cookson et al. 2005, Warner and Schapira 2003).

PD is typically diagnosed from the medical history of a patient and a neurophysiological examination (Jankovic 2008), and some institutions recommend periodical reviews of the diagnosis (National Collaborating Centre for Chronic Conditions 2006). An important tool to monitor the

patients response to L-3,4-dihydroxyphenylalanine (L-DOPA). L-DOPA is a precursor to dopamine able to cross the blood-brain barrier that is known to diminish symptoms of PD.

The mean age of onset for PD is ≈60 years, with a prevalence of 1 % of the population over 60 years of age and rising to 4 % in the population over 80 years. Overall prevalence in industrialized countries is around 0.3 % (de Lau and Breteler 2006, Samii et al. 2004).

There is currently no cure for PD, but several therapies exist that can relief the symptoms. On the pharmacological side, levodopa therapy is widely used (Birkmayer and Hornykiewicz 1998). Another option is surgery, where, due to its reversibility, deep brain stimulation (DBS) is often preferred over lesional surgery (National Collaborating Centre for Chronic Conditions 2006). DBS is a surgical procedure in which a so called brain pacemaker is implanted in the brain. Similar to the pacemaker used in heart diseases, it sends out electrical impulses to specific parts of the brain, which causes a mitigation of symptoms.

1.1.2 Dementia with Lewy bodies

DLB is the second most common degenerative dementia following Alzheimer's Disease (AD). Prodromal symptoms are cognitive impairment, behavioural/psychiatric phenomena like hallucinations and sleep disorder, and physical symptoms like parkinsonism and autonomic dysfunction (Donaghy and McKeith 2014). The cognitive impairment causes an outward similarity to AD which can lead to misdiagnosis. In fact, this similarity is also found on a biochemical level, as Lewy bodies are often found in the brain of patients with AD (Kotzbauer et al. 2001, Uchikado et al. 2006).

Currently there is no known cure for DLB and therapies purely aim to reduce the symptoms. Choice of therapies relies on the symptoms present in individual patients. Often, motor symptoms are treated with therapies used for PD, while cognitive impairment may be lessened by AD therapies.

1.1.3 Multiple-system atrophy

MSA is a synucleinopathy that causes a broad range of different symptoms, mainly categorized into three groups: autonomic failure, ataxia and parkinsonism. Symptoms can occur in any combination (Burn and Jaros 2001). A clear difference to other synucleinopathies is that the key α-synuclein aggregates of MSA, called glial cytoplasmic inclusions, occur in oligodendroglia instead of neurons (Papp et al. 1989). There is also significantly higher accumulation of α-synuclein in the brain (Chen

et al. 2014). Guidelines for clinical diagnosis were established in 1997 and reviewed in 2007 (Gilman et al. 1999, Gilman et al. 2008), but the only definite diagnosis remains the pathological detection of glial cytoplasmic inclusions (Papp et al. 1989). No cure is known for MSA, and treatment is aimed at helping patients cope with the numerous different possible symptoms.

1.2 α-synuclein

α-synuclein is a protein of 140 amino acids which was first identified in 1988 where it was found to be associated with cholinergic vesicles in the electric organ of the Pacific electric ray (*Torpedo californica*) (Maroteaux et al. 1988). Later, a 35 amino acid long sequence, found in amyloid preparations of Alzheimer's disease patients and labelled non-A-β-component (Ueda et al. 1993), was shown to be the analog human α-synuclein (Jakes et al. 1994).

The protein is located at the presynapse (Jakes et al. 1994, Iwai et al. 1995, Totterdell and Meredith 2005) where it was shown to interact with the membrane (Fortin et al. 2004, Chandra et al. 2005, Jo et al. 2004). Several studies have found a connection between α-synuclein on synaptic function either by influencing the vesicular pool (Cabin et al. 2002, Murphy et al. 2000), and it is also thought to play a role in neurotransmitter release (Lashuel et al. 2013) (Liu et al. 2004, Sidhu et al. 2004).

The primary amino acid sequence of α-synuclein can be divided into three main parts. The N-terminal region is amphipathic and contains imperfect 11 residue repeats. All known point mutation linked to familial forms of PD are found in this region. The central region is overall hydrophobic and contains the core region for fibril formation (Giasson et al. 2001). The C-terminal region is highly acidic and unstructured.

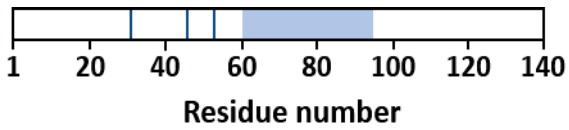

Figure 1: α-synuclein primary structure

Point mutations causing familial PD is shown in dark blue (residues 30, 46, 53). Central NAC region essential for aggregation is shown in light blue (Residues 60-95).

α-synuclein is a natively unfolded protein, as it shows no stable secondary structure in its monomeric form (Weinreb et al. 1996). There have been disputed reports claiming that a tetrameric

structure exists (Bartels et al. 2011). In disease associated inclusions like Lewy bodies and glial cytoplasmic inclusions α-synuclein adopts an aggregated, fibrillary form, which has been studied in detail (Heise et al. 2005).

1.2.1 Fibrillar structure of α-synuclein

The structure and formation of fibrils is a complex multi-step process that has been studied since the identification of aggregated α-synuclein in Lewy bodies. In general, soluble monomers assemble into metastable oligomeric intermediates which then form stable, fibrillar aggregates associated with cell death in synucleinopathies (Rochet et al. 2000, Uversky 2007). Formation of fibrils is nucleation dependent and the limiting factor in fibril growth kinetics is the spontaneous formation of the nucleus (Bhak et al. 2009, Li et al. 2009, Wood et al. 1999). Further fibril growth is mediated by a two-step mechanism. Monomers bind reversibly to fibrils, which causes an irreversible structural reorganization, integrating the monomer into the fibril and again presenting an interface for monomer binding (Collins et al. 2004, Esler et al. 2000). The mature fibrils are defined by a cross-β structure consisting of in register, parallel β-sheets. The side chains form a so called steric zipper, excluding water from the β-sheet interface (Nelson et al. 2005, Sawaya et al. 2007, Serpell et al. 2000). High resolution analysis of fibrils reveals structural polymorphism resulting in fibrils in either a straight or a twisted ribbon phenotype. Conditions during aggregation (pH, temperature, ion concentration, etc.) influence mature fibril structure (Heise et al. 2005, Vilar et al. 2008, Bousset et al. 2013).

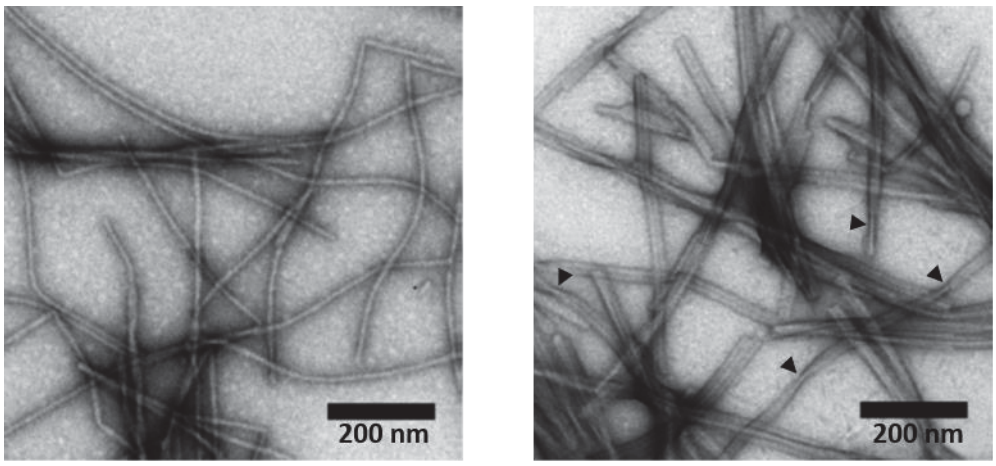

Figure 2: Negative stained TEM images of different fibril morphologies

Left: straight fibrils, right: twisted fibrils. Arrows mark the twists (Bousset et al. 2013).

1.2.2 Assessing conformational change during aggregation

Fibrillar growth is most commonly measured by fluorescence of Thioflavin T (ThT). ThT is a fluorescent dye that shows enhanced fluorescence as well as a characteristic red shift in contact with cross-β structures presented in fibrils. This effect is attributed to the accumulation and alignment of ThT molecules inside of groves between side-chains of the cross-β motif. This reduces intramolecular rotation of the excited state and thus increases fluorescence (Biancalana and Koide 2010). As increased fluorescence is dependent on cross-β structures it is only seen if fibrils are present, while monomers and oligomers do not exhibit any signal (Figure 3). The curve is typical for fibril formation. After a lag phase in which the fibrillation nucleus is formed, an exponential growth phase follows. At a certain concentration fibril growth stops and fluorescence reaches a plateau.

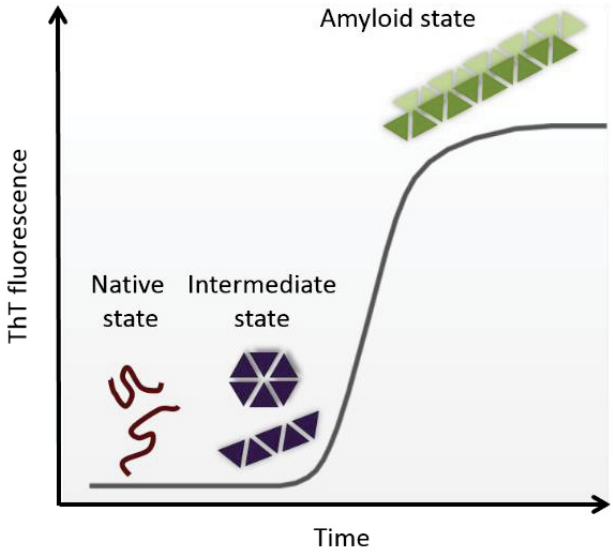

Figure 3: Example of fibril identification by ThT fluorescence

The ThT fluorescence is shown dependent on time. In the beginning, only monomers are in solution, which eventually form intermediate oligomers. Both do not exhibit ThT fluorescence. As soon as amyloid fibrils are formed, fluorescence of ThT rises.

Another sign of aggregation is the shift in secondary structure from the natively unfolded monomer to a β-sheet rich structure. This shift is often confirmed with Circular Dichroism (CD) spectroscopy. CD Spectra show the ellipticity of a sample in dependence of wavelength. Different secondary structure elements result in different spectra, which can be identified by analysing their extrema and zero crossing values.

1.2.3 Toxicity of α-synuclein

Toxicity of α-synuclein is linked to fibril formation, as fibrillar aggregates are found in Lewy bodies and glial cytoplasmic inclusions (Chapter 1.1, page 5). However, the mechanism behind the toxicity as well as the species mediating it are not well known. In recent years, most studies indicate that oligomeric species, not mature fibrils, may be responsible for cell death in synucleinopathies (Conway et al. 2000a, Conway et al. 2000b). A variety of morphologically different oligomeric species have been observed, preceding formation of fibrils *in vitro* (Horvath et al. 2012), as well as *in vivo* in diseased human brains (Baba et al. 1998, Kahle et al. 2001, Tsigelny et al. 2008).

The mutant A30P, a point mutation causing familial PD, shows increased oligomerisation, but not fibrillation *in vitro* (Conway et al. 2000a). Artificial mutations showing increased oligomerisation, but not fibrillation, are highly toxic to dopaminergic neurons in different animal models of synucleinopathies (Winner et al. 2011). In other work, oligomer forming mutations A56P and A30P/A56P/A76P were shown to have a high toxicity, but sustained, progressive loss of neurons was dependent on formation of mature fibrils, not oligomers (Taschenberger et al. 2012).

Considering the multitude of different intermediates formed in the aggregation process, it is likely that they contribute in separate ways to α-synuclein toxicity (Lashuel et al. 2013). Oligomers were shown to mediate toxicity by damaging mitochondria, causing lysosomal leakage or disturbing microtubules (Alim et al. 2004, Hashimoto et al. 2004, Hsu et al. 2000). They also interfere with synaptic transport of proteins, eventually causing neurodegeneration (Scott et al. 2010). Spherical oligomers with a diameter of 2-6 nm may contribute to toxicity by promoting neuronal degeneration and abnormal calcium currents in cultured neurons (Danzer et al. 2007)

1.3 α-synuclein as a biomarker for synucleinopathies

As mentioned before, clinical diagnosis of and differentiation between synucleinopathies is insufficient, due to the late onset of symptoms and similarities among the synucleinopathies themselves as well as between synucleinopathies and other neurodegenerative diseases like AD (Chapter 1.1, page 5). A reliable biomarker that supports clinical diagnosis is therefore of great importance. It could help identify diseases even before onset of symptoms, enabling new therapies and insights into disease progress. Such a biomarker should have high diagnostic sensitivity and specificity, and the collection should be reliable, reproducible, and simple to perform. It should also be validated by neuropathological inspection (Trojanowski and Growdon 1998).

α-synuclein is one such potential biomarker. It has been identified as a main component in Lewy bodies, the defining cellular inclusion for PD and DLB, and in glial cytoplasmic inclusions which are a hallmark feature of MSA (Baba et al. 1998, Wakabayashi et al. 2007, Spillantini and Goedert 2000). In the last decade several groups successfully detected full length α-synuclein in different biological fluids, including plasma and cerebrospinal fluid (CSF) (Mollenhauer et al. 2010). Decreased total α-synuclein was detected for both PD and MSA (Mondello et al. 2014, Wang et al. 2012), but similar concentrations did not allow a differentiation between both diseases (Aerts et al. 2012, Tateno et al. 2012). In general, decreased α-synuclein levels seem to indicate the presence of a synucleinopathy and thereby rule out other diseases with similar symptoms, but they are not yet sufficient to discriminate among synucleinopathies (Jimenez-Jimenez et al. 2014).

However, many of these results are based on the quantification of total α-synuclein concentration in CSF, and they do not consider the conformation of α-synuclein. Different studies have shown that the concentration in CSF increases if only oligomeric α-synuclein is measured (Park et al. 2011, Parnetti et al. 2014a, Tokuda et al. 2010, Parnetti et al. 2014b). This reveals the potential for aggregation-state sensitive detection methods to help establish α-synuclein as a biomarker.

1.4 Surface-based fluorescence intensity distribution analysis (sFIDA)

Immuonosorbent assays like ELISA (enzyme-linked immunosorbent assay) are often used to identify specific proteins in samples containing impurities and other proteins. They are both sensitive and specific to the overall concentration of protein, but they usually give no information on protein structure. One of the biggest disadvantages of using α-synuclein as a biomarker is that, as an endogenous human neuronal protein, its presence alone is not necessarily indicative of a disease. A common ELISA has been modified so that it does not recognise monomeric α-synuclein by using the same antibody for immobilisation and detection. Since both antibodies bind to the same epitope, monomers can only be bound either to the surface, giving no signal, or by a detection antibody, in which case they are removed by the washing steps (El-Agnaf et al. 2006). This way, the ELISA only detects dimers or higher oligomers.

sFIDA is an aggregate-specific immunosorbent assay developed at our institute that focuses on the detection and quantitation of protein aggregates (Birkmann et al. 2007). A sample is immobilised by capture antibodies on a glass surface, recognised by two detection antibodies each labelled with a different fluorescent dye, and images are recorded showing intensity distribution for each channel (Figure 4).

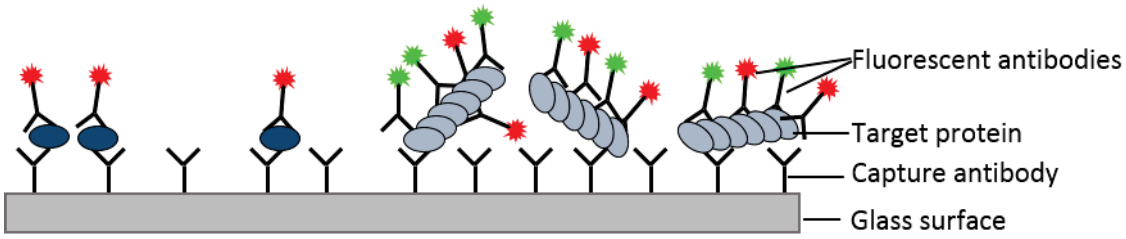

Figure 4: Setup of sFIDA assay

The capture antibody is covalently bound to the glass surface and binds protein close to the surface. Monomers (dark blue ellipses) and aggregates (rows of light blue ellipses) are immobilized. Fluorescently labelled detection antibodies bind to the protein. The same antibody is used as the capture and labelled with Alexa Fluor 488 (green marking), so monomers at the surface are only bound by detection antibody labelled with Alexa Fluor 633. Fibrils present many epitopes and are bound by several antibodies in each channel.

In the evaluation, images from both channels are combined into a single, colocalised image. In this process signal only present in one channel but not the other is disregarded. Therefore, signal from monomers that can only bind antibodies in a single channel is not carried over into the 2D image and aggregates are selectively detected. Larger aggregates will bind more antibodies at once and appear brighter then smaller aggregates or oligomers. The images also confer more information than just fluorescence intensity. The amount, size, brightness and distribution of aggregates can potentially be measured. This makes the sFIDA a very promising method for the detection and analysis of aggregated protein in body fluids, and possibly a powerful tool for biochemical diagnosis of protein misfolding diseases.

1.5 Aim of the thesis

The synucleinopathies are a group of age-related diseases that show a broad range of neurological symptoms caused by the death of neuronal cells. They are defined by inclusions of misfolded α-synuclein. Their clinical diagnosis is complicated and a definite diagnosis can only be made upon neuropathological examination. The symptoms occur many years after the actual onset of the disease, limiting therapeutic options to the treatment of symptoms. Identification of reliable biomarkers is of great importance as it would allow diagnosis at earlier stages of the disease. In this way, biomarkers would enable development of new treatments targeting not only the symptoms but the cause of the disease.

The level of α-synuclein in CSF is a promising biomarker for synucleinopathies, as not only total concentration but also aggregation state are thought to change during progression of PD, MSA and DLB.

The sFIDA is a sensitive fluorescence microscopy based immunoassay that specifically detects aggregated protein. It has been used in research on AD and prion diseases to identify aggregates of amyloid-β peptide or prion proteins, respectively.

The aim of this thesis was to develop the sFIDA assay for specific detection and quantitation of α-synuclein aggregates. This included production of recombinant human α-synuclein, establishing a method for preparation and storage of a-synuclein fibrils, optimisation of the antibody combinations used for immobilisation and detection as well as instrument settings and data evaluation. Finally, sFIDA was used for detection of a-synuclein aggregates in spiked CSF and samples from patients with synucleinopathies.

2 Materials and Methods

2.1 Materials and Chemicals

2.1.1 Buffers and Solutions

Table 1: Buffers and solutions

Lysogeny broth (LB)	10 g Tryptone, 5 g Yeast extract, 5 g NaCl, add 1 L H_2O
Ampicillin	100 mg/mL
Isopropyl-β-D-1-thiogalactopyranoside (IPTG)	1 M
IEC buffer A	20 mM Tris/HCl pH 7.7
IEC buffer B	20 mM Tris/Hcl pH 7.7, 1 M NaCl
Phosphate buffered saline (PBS)	1.33 g/L $CaCl_2$ $2H_2O$, 1 g/l $MgCL_2$, 2 g/L KCl, 2 g/L KH_2PO_4, 80 g/L NaCl, 11.5 g/L Na_2HPO_4
Phosphate buffered saline with Tween20 (PBST)	PBS, 0.1 % (v/v) Tween20
Tris buffers saline with Tween20 (TBST)	10 mM Tris/HCl pH 8.0, 150 mM NaCl, 0.01 % (v/v) Tween20
MES buffer for sFIDA	0.1 M MES, pH 7.7
Tris buffer	20 mM Tris pH 7.7, 150 mM NaCl
2-(N-morpholino)ethanesulfonic acid (MES) buffer	20 mM MES pH 6.0, 100 mM NaCl
NaP_i/SDS buffer	10 mM NaP_i pH 7.7, 100 mM NaCl, 0.5 mM SDS
Coomassie staining solution	0.2 % (w/v) Coomassie Brilliant Blue R250, 45 % (v/v) ethanol, 10 % (v/v) acetic acid
TGM buffer	25 mM Tris pH 8.3, 192 mM glycine, 20 % methanol

2.1.2 Antibodies

The following antibodies from Santa Cruz Biotechnology, Inc., Germany, were used.

Table 2: Antibodies

Name	Raised against	Use
211	Amino acids 121-125 of human α-synuclein	Western blotting, sFIDA
3H2897	Recombinant human α-synuclein	sFIDA
GaMPO	Conserved region of a mouse antibody	Western blotting

2.2 Recombinant expression of α-synuclein

2.2.1 Expression protocol

Human α-synuclein 1-140 was expressed in *E. coli* Bl21(DE3), containing the pt7-7 plasmid.

A pre-culture was prepared in a sterile 100 mL baffled flask containing 10 mL of LB medium with 100 µg/mL ampicillin (Table 1, page 14). A sterile pipet tip was scraped over the glycerol stock of *E. coli* and given into the solution. The flask was then placed in a shaker (Infors HT multitrion Standard, Infors AG, Switzerland) at 37 °C and 220 rpm overnight.

On the following day, 1 L of LB medium with a final concentration of 100 µg/mL ampicillin was prepared in a sterile 2 L baffled flask. The pre-culture was decanted into this solution, and the 2 L flask placed back in the shaker at 37 °C and 220 rpm. The optical density (OD) at 600 nm was measured (OD600 DiluPhotometer, Implen GmbH, DE) every 20 min. Upon reaching an OD_{600} of 0.6, expression of α-synuclein was induced by addition of IPTG at a final concentration of 1 mM (Table 1, page 14). After 4 h, cells were harvested by centrifugation at 3000 x *g* (Centrifuge: X-15R, Rotor: SX4750A, BeckmanCoulter GmbH, DE). Cell pellets were stored at -20 °C or used immediately.

2.3 Purification of recombinant α-synuclein

After expression, the α-synuclein is still contained within the *E. coli* cells. To obtain the protein in a concentrated and pure solution, the following purification method was used.

2.3.1 Cell lysis

The cell pellet obtained during the expression of α-synuclein (Chapter 2.2.1, page 15) was thawed by shaking at 4 °C in 5 mL Tris buffer (Table 1, page 14) containing one tablet of protease inhibitor (cOmplete mini EDTA free tablets, F. Hoffmann-La Roche AG, CH) for 20 min. Subsequently, the cells were resuspended by pipetting with an automatic pipette (Pipetboy acu 2, VWR, Germany). Cell lysis was achieved by using a cell disrupter (One Shot model, Constant Systems Ltd., UK) at 2.5 kbar.

2.3.2 Thermal denaturation

After lysis of the cells, α-synuclein is in solution, but still contaminated with other proteins, nucleic acids and lipids. As a first step to purify the protein, the solution was heated immediately for 10 min at 95 °C in a heat block. Afterwards, the solution was centrifuged for 30 min at 4 °C and 13000 rpm (Centrifuge: J2-21, Rotor: Ja 20.1, BeckmanCoulter GmbH, Germany). The pellet was discarded and the supernatant containing the thermostable and thus still soluble α-synuclein was used for further purification.

2.3.3 Ammonium sulphate precipitation

Following thermal denaturation and separation from insoluble impurities by centrifugation, an ammonium sulphate precipitation was carried out with the supernatant to separate α-synuclein from remaining soluble impurities. The solution was kept on ice and agitated with a magnetic stirring bar. 0.45 g/mL ammonium sulphate was added over a period of 10 minutes. After 1 h of stirring, the solution was centrifuged for 30 min at 4 °C and 13,000 rpm (Centrifuge: J2-21, Rotor: Ja 20.1, BeckmanCoulter GmbH, Germany). The supernatant was discarded and the pellet used for further purification steps.

2.3.4 Ion exchange chromatography (IEC)

The pellet from the ammonium sulphate precipitation (Chapter 2.3.3, page 16) was resuspended in 50 mL of IEC buffer A (Table 1, page 14) and further purified via ion exchange chromatography, using a HiTrap Q FF column with 5 mL volume (GE Healthcare Europe GmbH, Germany) connected to an ÄKTApurifier liquid chromatography system (GE Healthcare Europe GmbH, Germany).

The sample was applied with a flow rate of 2 mL/min and washed with 12 column volumes of IEC buffer A (Table 1, page 14) to remove unbound proteins from the column. For elution, a gradient of 0-500 mM NaCl was used by dilution of IEC buffer B (Table 1, page 14).

The absorption was measured at 275, 254 and 215 nm to detect aromatic amino acids, nucleic acids and peptide bonds, respectively. The run was fractionated using the Frac-950 module for the ÄKTApurifier. Fractions showing a peak in absorbance at 275 nm at ≈300 mM NaCl were pooled and used for further purification steps.

2.3.5 Size exclusion chromatography (SEC)

The samples obtained from the ion exchange chromatography (Chapter 2.3.4, page 17) were used in a final purification step by size exclusion chromatography, using a Superdex 75 10/300 GL column (GE Healthcare Europe GmbH, Germany) connected to the ÄKTApurifier system.

SEC was carried out with a flow rate of 1.5 mL/min for 25 mL.

Fractions constituting a peak of absorbance at 275 nm were collected and pooled.

2.4 Determination of protein concentration by absorption spectroscopy

The concentration of α-synuclein in solution was determined by absorption spectroscopy. A spectrum from 220-320 nm was measured using a Jasco V-650 spectrometer (Jasco Germany GmbH, Germany). The concentration was calculated using the equation derived from the Lambert-Beer Law

$$A = c * \varepsilon * d$$

A is the absorption at a specific wavelength, c is the concentration, ε is the molar extinction coefficient at the measured wavelength and d is the length of the light path).

The absorbance at 275 nm, correct for the baseline at 320 nm, and a molar extinction coefficient of ε_{275}=5,600 M^{-1} cm^{-1} (Hoyer et al. 2002) were used in the calculation.

2.5 Determination of concentration of aggregated α-synuclein by absorption spectroscopy

The concentration of aggregated protein cannot be measured directly by absorption spectroscopy because aggregates might diffract light or sediment to the bottom of the cuvette and thus not remain in the light path. Therefore, concentration of aggregates was determined indirectly. Aggregated protein was removed from the sample by centrifugation for 100,000 x *g* at 4 °C for 1 h. The concentration of remaining monomeric α-synuclein in the supernatant was measured as described in chapter 2.4. The difference between monomer concentration and initial concentration equals the amount of aggregated protein.

2.6 Gel electrophoresis and protein staining

Gel electrophoresis is a common and widely used method for protein separation. Driven by an electric field, proteins travel at specific speeds through a gel matrix, concentrating in bands, depending on their size and charge. Their size is estimated by comparison to a marker containing proteins of known size. After separation, proteins are either stained directly and unspecifically by Coomassie Brilliant Blue staining, or transferred onto a membrane by blotting and identified by immunostaining.

2.6.1 Denaturing gel electrophoresis (SDS-PAGE)

Sodium dodecyl sulphate polyacrylamide gel electrophoresis (SDS-PAGE) is a common technique of protein gel electrophoresis. By heating in presence of SDS, proteins lose all secondary and tertiary structure elements and their native charge is overlaid by the negative charge of SDS. In consequence, different proteins are only separated by size, independently from both structure and charge.

Compositions of resolving and stacking gels are listed in Table 1. Buffer for stacking gels was 0.5 M Tris/HCl pH 6.8, resolving gels were buffered with 1.5 M Tris/HCl pH 8.8.

Table 3: Composition of gels for SDS-PAGE

	H_2O (mL)	**30 % Acrylamide/Bis (mL)**	**Buffer (mL)**	**10 % (w/v) SDS (mL)**
Stacking gel (5 %)	5.7	1.7	2.5	0.1
Resolving gel (15 %)	2.4	5	2.5	0.1

For polymerisation of the acrylamide, 50 µL of 10 % (w/v) ammonium persulfate and 5 µL TEMED were added to both stacking and resolving gel.

Gels were run for 45 min at 180 V in a Mini-PROTEAN Tetra Cell electrophoresis chamber (Bio Rad GmbH, Germany)

2.6.2 Coomassie Brilliant Blue protein staining

To stain protein bands, Coomassie Brilliant Blue staining was used. After electrophoresis was complete, the resolving gel was submerged in Coomassie staining solution (Table 1, page 14) for 15 minutes. Subsequently, gels were destained in H_2O until the clear of unspecific background staining.

2.6.3 Western blotting and immunostaining

To specifically identify α-synuclein after a SDS-PAGE, western blotting was performed as follows:

- Cut six pieces of Whatman paper and one piece of PVDF membrane in the size of the gel
- Soak Whatman paper and gel in TGM buffer (Table 1, page 14)
- Activate PVDF membrane with ethanol and soak in TGM buffer separately
- Place components into drawer of TransBlot Turbo instrument (Bio-Rad Laboratories GmbH, Germany) in this order:
    - 3x Whatman paper
    - PVDF membrane
    - Gel

    - 3x Whatman paper
- Blot for 30 min at 25 V and 1 A
- Block membrane for 1 h with 5% (w/v) milk powder in TBST
- Wash 3x for 10 min in TBST
- Incubate for 1 h in 20 mL antibody 211 diluted in PBS to a final concentration of 400 ng/mL
- Wash 3x for 10 min in TBST
- Incubate with GaMPO antibody diluted 1:10,000 in PBS for 1 h
- Wash 3x for 10 min in TBST

Detection was done using a ChemiDoc MP gel documentation device (Bio-Rad Laboratories GmbH, Germany) and the SuperSignal West Pico Chemiluminescence Kit (Thermo Fisher Scientific Inc., Germany).

2.7 Aggregation of α-synuclein

The aggregation of α-synuclein was carried out in different condition detailed in Table 4.

Table 4: Conditions of α-synuclein aggregation

Volume (µL)	α-synuclein (µM)	Buffer
350	150	20 mM Tris pH 7.7, 150 mM NaCl
350	150	20 mM MES pH 6.0, 100 mM NaCl
350	70	10 mM NaP_i pH 7.7, 100 mM NaCl, 0.5 mM SDS

Aggregation of α-synuclein was performed in 2 mL glass vials (Zinsser Analytic GmbH, Frankfurt, Germany) at 37 °C under agitation from a magnetic stirring bar. The vials were sealed with screw tops containing a PTFE septum to prevent evaporation.

2.8 Biophysical characterisation of α-synuclein aggregate formation

During and after maturation of the fibrils, biophysical properties of the protein were measured, to assess the change in structure.

2.8.1 Circular dichroism (CD) spectroscopy

The change of secondary structure during aggregation was measured using CD spectroscopy. For each measurement, 10 µL of the α-synuclein solution were diluted 1:10 in the respective buffer. The measurement was carried out in a Jasco J-815 CD Spectrometer (Jasco Germany GmbH, Germany) according to the parameters detailed in Table 5.

Table 5: Parameters for CD – spectroscopy measurements

Wavelength	260 – 190 nm
Data pitch	0.5 nm
Scanning Speed	100 nm/min
Scanning Mode	Continuous
Response	2 s
Bandwith	1 nm
Accumulations	20

Resulting spectra were classified by comparing their defining features (extrema and zero-crossing point) with standard spectra of the specific secondary structures.

2.8.2 Thioflavin T (ThT) fluorescence assay

ThT is a fluorescent dye commonly used to identify amyloid aggregates. Upon binding to such aggregates, the dye displays a characteristic increase in fluorescence as well as a redshift. By measuring the fluorescence of the samples during aggregation (Chapter 2.7, page 20), the formation of amyloid aggregates is monitored in a time dependent manner.

A volume of 3 µL of the α-synuclein stock solution (Table 4, page 20) was diluted 1:50 of the respective buffer, additionally containing ThT at a final concentration of 10 µM. An emission spectrum was measured in a Jasco FP-6500 Spectrofluorometer (Jasco Germany GmbH, Germany) according to the parameters detailed in Table 6.

Table 6: Parameters for the measurement of ThT fluorescence

Excitation	446 nm
Emission	465 – 600 nm
Bandwith (Excitation/Emission)	5 nm
Sensitivity	Medium
Data pitch	1 nm
Scanning Speed	200 nm/min
Accumulations	10

2.8.3 Atomic force microscopy (AFM)

The atomic force microscopy allows the capturing of high-resolution pictures on a nanometre scale. The sample is immobilised on a surface, which is then scanned by a cantilever. Deflection of the cantilever is measured and gives information on the height of any object at this position compared to the surface.

Samples containing 50 µL of a 5 µM α-synuclein solution were adsorbed on a fresh mica surface (JPK Instruments AG, Germany) for 1 h, followed by two washing steps with 200 µL water each. The sample was measured in a JPK Nano Wizard II microscope using a silicon OMCL-AC160TS cantilever (Olympus Deutschland GmbH, Germany) with a silicon tip (radius 9 ± 2 nm). Imaging was carried out in intermittent contact mode.

2.9 Fluorescent labelling of antibodies

To enable the specific detection of α-synuclein aggregates by fluorescence microscopy, commercially available antibodies were labelled with the fluorescent dyes Alexa Fluor 488 and Alexa Fluor 633.

2.9.1 Labelling of antibodies with Alexa Fluor 488

Antibodies were labelled with Alexa Fluor 488 fluorescent dye with the Alexa Fluor 488 Antibody Labelling Kit purchased from Life technologies (A-20181, Life technologies GmbH, Germany).

A solution with a volume of 100 µL was prepared by mixing the 50 µg of the antibody with the required amount of H_2O, depending on the antibody concentration, and then adding 10 µL freshly

prepared 1 M $NaHCO_3$. This mixture was transferred to the vial containing the dye, inverted several times, and stored at 4 °C over night in the dark.

On the following day, purification of the antibody, determination of concentration and calculation of the degree of labelling were carried out according to the manual.

Finally, to stabilise the antibodies during storage at 4 °C, an equal volume of PBS buffer containing 3 % bovine serum albumin was added to the samples.

2.9.2 Labelling of antibodies with Alexa Fluor 633

Labelling antibodies with AlexaFluor633 was done with the Alexa Fluor 633 Protein Labelling Kit (A-20170, Life technologies GmbH, Germany).

The dye was solubilised in 100 µL H_2O. A solution with a volume of 100 µL was prepared, containing 50 µg of the antibody, the required amount of H_2O depending on the concentration of the antibody, 10 µL of the dye solution and, added last, 10 µL 1 M $NaHCO_3$. The solution was stored in the dark at 4 °C over night.

Purification was carried out according to the manual of the kit used for labelling antibodies with Alexa Fluor 488 (Chapter 2.9.1 page 22). Determination of the protein concentration and calculation of the degree of labelling were done as described in the manual of the Alexa Fluor 633 Labelling Kit.

To stabilise the antibodies during storage at 4 °C, an equal volume of PBS buffer containing 3 % bovine serum albumin was added to the solution.

2.9.3 Surface plasmon resonance (SPR) measurements of labelled antibodies

SPR is a method that uses the conversion of energy from incident light into surface plasmons as a way of detecting changes in the surrounding medium. In the BIAcore setup, these changes can be used to accurately calculate binding kinetics between molecules.

The general setup of a SPR chip consists of a glass surface coated with a gold film and a flow cell on the other side. Light is directed through the glass at the gold in such a way that total internal reflection occurs. The angle of the light is shifted and the intensity is recorded for each angle. At a certain position, the SPR angle, no light is reflected although total internal reflection should still occur. This is due to the formation of surface plasmons. Surface plasmons are electron density waves that are created by the incident light and propagate along the surface of the gold layer.

Under steady conditions they have a specific momentum vector parallel to the surface. The momentum of photons reflected at the surface can be expressed as one vector perpendicular to the surface and one vector parallel to it. If the parallel momentum vector of the photon and the plasmon are equal, the energy of the photon is converted into plasmons and ultimately dissipated as heat. Therefore, no light is reflected at this specific angle. A change in the medium above the gold layer influences the momentum vector needed to create surface plasmons and in consequence leads to absorption of light at a different angle.

In praxis, one molecule, called ligand, is immobilised on the surface while its potential binding partner, called analyte, is carried over the chip with a steady flow of buffer. The change in SPR angle caused by binding of the analyte is recorded as a function of time and used to calculate parameters of binding kinetics.

Here, SPR was used to determine the affinity of antibodies to α-synuclein, and to check if those affinities are affected by the fluorescent labels attached to them (Chapter 2.9, page 22). The measurements were done in a BIAcore T200 (GE Healthcare Europe GmbH, Germany). A CM5 sensor chip was prepared by binding α-synuclein fibrils matured in the NaP_i/SDS system (Chapter 2.7, page 20) to the surface using the Amine Coupling Kit (GE Healthcare Europe GmbH, Germany). The analyte was prepared in five different concentrations. Following the injection of 180 s, dissociation was monitored for 420 s at a flow rate of 30 mL/min and a temperature of 25 °C. The running buffer was 10 mM HEPES, pH 7.4, 150 mM NaCl, 3 mM EDTA and 0.005 % (v/v) Tween 20. For each measurement, the signal of an uncoated reference cell and the signal generated by injection of running buffer was subtracted from the sensorgrams. Data was analysed using the BIAcore T200 evalutation software.

2.10 Surface-based fluorescence intensity distribution analysis (sFIDA)

sFIDA is a method developed to specifically detect and quantify aggregated protein by fluorescence microscopy. An antibody is covalently bound to the surface of a glass-bottom multiwell plate via a spacer molecule, based on a protocol published by Janissen *et al*. (Janissen et al. 2009). This antibody is called the capture antibody. When a sample is brought onto the surface and washed off again, only protein that can be bound by the capture antibody remains. To detect the bound protein, two fluorescently labelled antibodies, each with a specific epitope and labelled with different fluorescent dyes, are applied. The surface is then imaged by dual-colour fluorescence microscopy. Only colocalised signals above an intensity threshold are evaluated (Chapter 2.11, page

32). This diminished false positive signal, for example from a cross reactivity of the antibody in one channel. By using the same antibody as capture and as one of the detection antibodies the detection of monomers is excluded as monomers have only a single epitope and so cannot be bound by the capture and the detection antibody at the same time.

2.10.1 Preparation of the surface

The following procedure was used to prepare 384-well plates with a 170 µm glass bottom (Greiner Bio-One International GmbH, Austria). Pipet tips were placed in the lower right hand corner of each well, while not touching the surface to avoid scratching. Washing steps consisted of gently pipetting all of the solution up and down three times, and typically repeated 3 times.

First, the wells need to be cleaned, to remove any possible contamination, for example dust or organic components. This was done by incubation first with 5 M NaOH, followed by incubation with 1 M HCl.

Cleaning of the wells

- Incubate with 100 µL 5 M NaOH for 15 min
- Wash with 3x100 µL H2O
- Incubate with 100 µL 1 M HCl for 15 min
- Wash with 3x100 µL H2O
- Wash with 2x100 µL Ethanol
- Dry with N2 gas stream

Afterwards, the glass surface was activated to prepare the binding of the NHS-PEG-COOH spacer (MW 3,400, Laysan Bio, USA). Ethanolamine was dissolved in DMSO (0.55 g/mL) at 70 °C, degassed for 30 min using 3 Å molecular sieve beads and left to react on the surface overnight. The ethanolamine is bound to the silanol groups of the glass.

Activation of the glass surface

- Incubate with 20 µL Ethanolamine over night
- Wash with 3x100 µL DMSO

- Wash with 2x100 µL Ethanol
- Dry with N2 gas stream

In the next step, the PEG spacer was bound to the amino groups of the activated glass surface. 17 mg NHS-PEG-COOH were dissolved in 100 µL DMSO at 60 °C and left to cool. After reaching ambient temperature, 2 µL triethylamine were added. The sulfo-N-Hydroxysuccinimide (NHS) binds the spacer to the amine group of the ethanolamine, covalently linking it to the surface.

Application of the PEG spacer

- Incubate with 15 µL PEG/triethylamine for 1 h
- Wash with 3x100 µL H_2O

Following the binding, the spacer was activated. NHS and 1-Ethyl-3-(3-dimethylaminopropyl)-carbodiimide (EDC) were dissolved in MES buffer (Table 1, page 14) at the concentrations of 11.6 mg/mL and 19.2 mg/mL respectively. Both solutions were mixed 1:1 directly prior to application. This activates the carboxylic group of the PEG spacer and prepares binding of the antibody.

PEG activation by NHS/EDC

- Incubate with 30 µLNHS/EDC for 45 min
- Wash immediately with 3x100 µL MES

Following this step, the capture antibody was bound covalently to the spacer by a peptide bond between free amino groups on the protein and the activated carboxylic group on the spacer. The antibody was applied at a concentration of 50 ng/µL in PBS (Table 1, page 14). From here on, PBST (Table 1, page 14) was used in the first washing step. Tween20 functions as a detergent and allows a more stringent cleaning than pure buffer. The second washing step was done with PBS to remove Tween20 from the well.

Binding of the capture antibody

- Incubate with 15 µL diluted antibody for 1 h
- Wash with 3x100 µL PBST
- Wash with 3x100 µL PBS

In the next step, the remaining free glass surface is blocked with bovine serum albumin to prevent unspecific binding of the sample or the detection antibodies to the glass surface.

Blocking the free surface

- Centrifuge 3 % bovine serum albumin solution at 100,000 x *g* for 1 h at 4 °C
- Incubate with 50 µL over night
- Wash with 3x100 µL PBST
- Wash with 3x100 µL PBS

Now the target can be applied to the prepared surface. The plates are centrifuged at 1000 x *g* to enhance sedimentation of aggregated proteins. The temperature is kept at 25 °C so the binding of the capture antibody and α-synuclein is not impaired.

Binding the Target

- Incubate with up to 100 µL of the target for 1 h at 1000 x *g* at 25 °C
- Wash with 3x100 µL PBST
- Wash with 3x100 µL PBS

In the last step, the detection antibodies are applied. Prior to this they are centrifuged to sediment any aggregates that may have formed during storage, and only the supernatant is used. Aggregates of fluorescently labelled detection antibodies might be incorrectly identified as α-synuclein aggregates if they are found during the measurement.

Application of detection antibodies

- Prepare a solution containing 2 ng/µL of both detection antibodies and centrifuge at 100,000 x *g* at 4 °C for 1 h
- Incubate wells with 15 µL of the supernatant for 1 h
- Wash with 3x100 µL PBST
- Wash with 3x100 µL PBS

2.10.2 Measurement by total internal reflection fluorescence microscopy (TIRFM)

TIRFM is a specific type of fluorescence microscopy used to excite fluorophores in a very thin layer atop a glass surface.

Total internal reflection can occur when light strikes a boundary of two materials with different refractive indices. Usually, light will be partially refracted and partially reflected in such a case. However, if the refractive index is lower beyond the boundary and the light exceeds a certain critical angle, the beam does not pass the boundary but is reflected completely.

In TIRFM, this is realised by directing a laser through the objective at a glass surface in such a way that the critical angle is exceeded. To ensure that the reflection takes places at the boundary between glass surface and the sample, and not at the lens of the objective, immersion objectives are used combined with an immersion liquid of the same refractive index as glass.

Total internal reflection causes an evanescent wave on the far side of the boundary. This wave has the same wavelength as the reflected beam, but is subject to an exponential decay of intensity with increasing distance to the surface. In practise, the continuous laser beam creates an evanescent field which illuminates a layer with a thickness of a few hundred nanometres, approximately $^1/_3$ λ. Only fluorophores within this layer are excited. This can greatly reduce background fluorescence, improving the signal-to-noise ratio in the images.

The microscope used was a Leica AF6000LX inverted microscope with a HCX PL APO 100x 1.47 oil objective, controlled by the LAS X software (Leica Microsystems GmbH, Germany). Images were recorded with an EM-CCD camera (Digital camera C9100, Hamamatsu Photonics Deutschland GmbH, Germany). The settings of the software are detailed below.

- Start the Software
- Select following options: Configuration: Dynamic Widefield Tree; Microscope: Dynamic

- Start MatrixScreener module
- Select Application: Load template “384 Sensoplate Greiner Bio one (Steffen) 9x6” to define coordinates of the plate in relation to the microscope table
- Change active tab to “Adjust Experiment”
- Select “Collecting pattern” and load parameter file “ElkesImagingPattern”
- Select “AF job” and load parameter file “ElkeC” to set parameters for the autofocus job
- Set autofocus to “continuous” and manually focus on the surface. Then click “Store AFC Position” and “Hold AFC” to save the z-coordinates of the surface
- Switch to “Imaging pattern” and load parameter file “ElkesI” to set the parameters of the imaging job
- Manually focus on the surface in each channel of the imaging job. Then click “Store AFC Position” and “Hold AFC” to save the z-coordinates of the surface for each channel
- Switch to “Collecting pattern”
- Change active tab to “Adjust sample”
- Select “Centralize well” and follow the instructions
- Select wells to be measured
- Move to the middle of the first well and manually adjust focus. Select “set z to all fields” and “set z to current well”
- Cycle through all wells and manually adjust focus in each one. Select “set z to well” each time
- Move to the first well. Adjust focus, press “DFC hold”.
- Press “Run matrix”

Each image has a resolution of 1000x1000 pixels and depicts an area of 114.17x114.17 µm, giving each pixel the dimension of 114x114 nm. To automate the measurement, a template was defined so that in each well, a matrix of 6x9 areas was imaged in two channels, recording fluorescence of Alexa Fluor 633 and Alexa Fluor 488, respectively. The detailed parameters for both channels are listed in Table 7. Images were exported as in the .tiff format and further analysed using a script for the image processing program ImageJ as described in Chapter 2.11.

Table 7: Parameters of TIRFM channels

	Channel 1 (Red)	Channel 2 (Green)
Excitation wavelength	635 nm	488 nm
Laser intensity	80 %	100 %
Penetration depth	250 nm	250 nm
Exposure time	300 ms	300 ms
EM Gain	800	1200
Emission filter	BP705/72	BP525/36

2.10.3 Measurement by confocal laser scanning microscopy (CLSM)

CLSM is a type of fluorescence microscopy which allows to take images with a defined and limited depth-of-field. Typically, a laser is focused on the sample volume through a lens after passing a dichroic mirror. The fluorescence from the sample is reflected by the mirror onto the detector. In front of the detector is a very small aperture, the so called pinhole, which lets only the light emitted at the focal point through while blocking out all light that originated above or below it. The light detected constitutes one pixel of the final image. The laser scans the sample pixel by pixel and line by line, creating a complete image.

The images were recorded on a Leica TCS SP5 II (Leica Microsystems GmbH, Germany). Fluorescence was recorded using HyD detectors in photon counting mode The settings of the software are detailed below.

- Start Leica LAS X software
- Select the following options: Configuration – machine without Obj Micro Pump, Microscope Stand – DMI6000, Resonant scanner not activated
- When prompted, allow initialization of the DMI6000 stage
- In the software, select “Configuration”, then select “Laser”
- Activate the argon laser, set the intensity to 30 %. Activate the HeNe633 laser
- Start the MatrixScreener software module
- Select “MatrixScreener Configuration”. Change to the “LIF Converter Settings” tab. Define folders and paths for the data of the experiment
- Switch back to “MatrixScreener Applications”. Select “Multiple regular matrices”

- Switch to the “Setup Template” tab
- Select template “cwd_disaster” to define coordinates of the wells in relation to the microscope table
- Right click onto the template and choose “Adjust well center – rectangular wells” from the context menu to precisely calibrate the coordinates of the reference well B2
- Switch to the “Setup jobs” tab
- Go to “2D Job” and find the “Sequential Scan” window under “Acquisition”. Load Settings “Steffen2D”. This loads the parameters for both channels, detailed in Table 8.
- Select “Autofocus job” tab, and set the autofocus to “On demand” mode
- Manually find the surface either by eye, using the objective and the I3 light source, or by performing a xz scan using the software
- Once the surface is in focus, pess “Set Experiment Position” and “Store AFC Position”
- Change to the “Setup Experiment” tab
- Select “Synchronize all z-Positions of all Jobs”
- Switch back to the “Setup Jobs” tab and ensure that the z-Position of the 2D Job has been change to the value of the Autofocus Job
- Switch again to the “Setup Experiment” tab
- Select which wells should be measured through “Delete Selection” and “Assign Scan Job”
- Press the “Autofocus Map” button to generate a map of the respective z-Position for each well. The instrument will scan trough the selected wells line by line. If a correct z-Position is found within the autofocus range, a green light will appear. A red light indicates that no autofocus position has been found for this well. If for one or more wells no autofocus position could be found, either repeat the scanning of the autofocus map, or manually find the correct position in each well in. Select “Set z-Position to well”
- Manually move the table to the first well and press “Start measurement”

In each well, a matrix of 5x5 images were taken. At a resolution of 2048x2048 pixels and a physical size of 247.6x247.6 µm for each area, each pixel has a dimension of 121x121 nm.

Table 8: Parameters of the settings for the 2D Job "Steffen 2D"

	Channel1	Channel2
Excitation wavelength	633	488
Laser intensity	25 %	25 %
Emission spectrum	639-769 nm	491-614 nm
Resolution	2048x2048	2048x2048
Size of imaged area	247.6 x 247.6 µm	247.6 x 247.6 µm
Scanning speed	600 Hz	600 Hz
Line average/ Line accumulation	3/1	3/1
Frame average/ Frame accumulation	1/1	1/1

2.11 Evaluation of sFIDA measurements

In sFIDA measurements, a large number of images is acquired. Depending on the sample size, several thousand images are common. Analysis and comparison of these images manually is very inefficient and time consuming. In this work, evaluation was automated using a script for the imaging processing software ImageJ described below.

2.11.1 Colocalisation of images

The sFIDA measurements detailed in chapters 2.10.2 and 2.10.3 produce separate images for the fluorescence of Alexa Fluor 488 and Alexa Fluor 633, showing the distribution of the respective fluorescence over a specific area. The images for each area are colocalised using the LeicaColoc_v1.25 script written by Fabian Dreßen (Institut für Physikalische Biologie, Heinrich-Heine-Universität Düsseldorf) for the imaging processing software ImageJ. Colocalisation is realised by multiplication of the grey values of each pixel, giving the grey value for the corresponding pixel in the colocalised image (Figure 5).

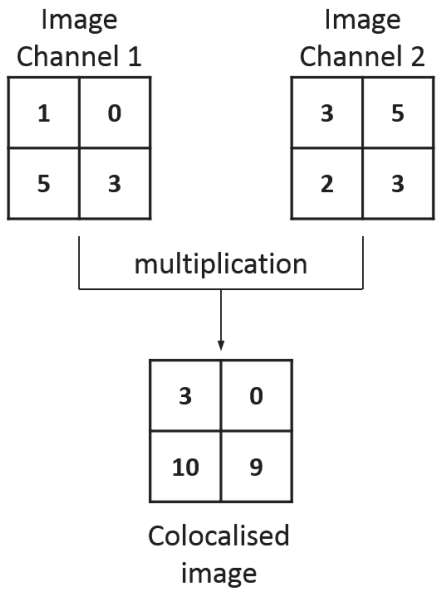

Figure 5: Concept of the colocalisation process

An example for the process of colocalisation. Two single channel images of 2x2 pixels each are colocalised into a single image of the same dimension by multiplication. Number represent intensities of single pixels. Positive signal in both channels is increased (lower two pixels) or retained (upper left pixel). If no signal is present in one of the channels, the colocalised image also shows no signal (upper right pixel)

The multiplication operator works in two ways. First, it increases the signal-to-noise ratio by increasing a moderate to strong signal present in both channels more than a low signal. Large aggregates are labelled with several antibodies at once, resulting in a local, high fluorescence peak, while background noise usually consist of evenly distributed light of a low intensity. Secondly, it excludes signal which is only present in one channel, because the signal will be multiplied with a grey value of zero from the other channel, resulting in a value of zero for the colocalised image. This effect is depicted in the upper right pixel in Figure 5.

2.11.2 Outlier test

One important aspect of the analysis is to decide which images are used for further analysis, and which are to be excluded. A measurement typically includes a small amount of pictures that show artifacts from preparation, for example bubbles or scratches on the surface, or that are completely black as a consequence of focus loss during automated image acquisition. Incorporating these images in any further analysis have considerable effect on the results, as the fluorescence in these pictures is not corresponding to the amount of labelled aggregates.

One possible method to identify those images would be to manually look through all images and decide which images should be excluded. However, this method is fairly time consuming and hard to automate. Most importantly the method is prone to variation due to subjective evaluation by different experimentators. The results for the same set of data might vary depending on the person carrying out the analysis, depending on which images will be considered to be erroneous. To avoid these problems, in this work the images were categorized and analysed by a simple statistical tool. The intensities of each pixel for each image were added up, giving a single value representing total fluorescence intensity. The standard score was calculated by taking each value, subtracting the mean of all images in this well and dividing the result by the standard deviation:

$$z = \frac{x - \mu}{\sigma}$$

z is the standard score, x is the raw score of the sample, μ is the mean of the population and σ is the standard deviation of the sample.

This results in a single, dimensionless value for each image that represents its distance to the population mean in standard deviations. A high score indicates a large distance between the value and the mean, with positive values being above the mean and negative values below.

All images with $z < -2$ or > 2 were considered as outliers and excluded from further analysis. Colocalised images were excluded if either the image itself or at least one of the single channel images they were calculated from were considered outliers

2.11.3 Cutoff determination

Images acquired by fluorescence microscopy often show a low but measureable background noise. The background is homogeneously distributed, so it can be considered to contribute equally to the value of each single pixel. This is a problem that becomes more important in sFIDA measurements the lower the amount of aggregates in the sample is. If a negative control containing no aggregates is compared to a sample containing a small number of aggregates, the difference in fluorescence might not be recognisable if the background is too high. A cutoff can be used to increase the signal-to-noise ratio by subtracting the background intensity from each pixel. This is depicted in Figure 6.

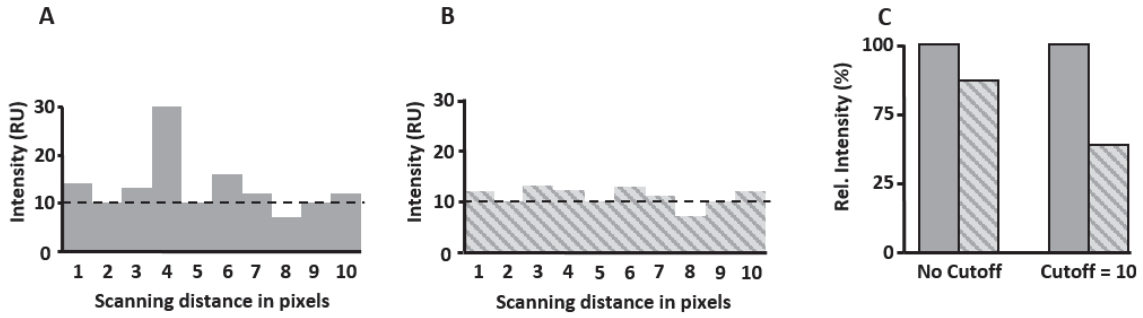

Figure 6: Exemplary illustration of the cutoff

Figures A+B show the intensity of 10 pixels. In Figure A, a single positive signal is recorded at pixel 4, above the background of the other pixels, exemplary for detection of single aggregates in sFIDA. In Figure B, only background noise is recorded, representing a negative control without aggregates. Figure C shows the sum of pixel intensities as percentage of the signal from the positive sample without a cutoff (dark grey bar) and with a cutoff at 10 RU (light grey striped bar).

It becomes clear that, while lowering overall signal, the cutoff increases signal-to-noise ratio.

In this work, the cutoff was determined in a simple but effective and reproducible way. It was calculated based on the relevant negative control for each samples. First, the standard score was calculated (Chapter 2.11.2, page 33). All images with a standard score between 2 and -2 were loaded into ImageJ. A histogram based on all images was calculated and the cutoff value was set as the mean plus three standard deviations from this histogram.

The cutoff for each sample was set separately for each channel, and colocalisation was calculated after its application.

2.11.4 Evaluation of TIRFM measurements

Cutoff values were determined according to chapter 2.11.3 and subsequently entered into the colocalisation script. In the resulting file, the standard score of each image was calculated separately for each well and each channel. All values <-2 and >2 were excluded and the mean of the remaining values was calculated. The mean values of different samples were presented in a bar chart and compared.

2.11.5 Evaluation of CLSM measurements

The HyD detectors of the CLS microscope were used in photon counting mode. The signal was not amplified in the detector, each measured photon was counted as a single event. Resulting

intensities for the pixel represent the number of events counted during the measurement. This sensitive detection mode creates images in which no signal is recorded for most of the pixels. Therefore, the cutoff value calculated as described in chapter 2.11.3 was not needed. Instead, the evaluation was done directly with the raw data.

The intensities for all areas were calculated using the LeicaColoc_v1.25 script (Chapter 2.11.1, page 32). A standard score was determined for the images in all three channels and all wells separately (Chapter 2.11.2, page 32) and all values not between 2 and -2 were removed. The mean of the remaining values was compared between samples.

3 Results

3.1 Production of α-synuclein

In order to establish the measurements of α-synuclein aggregates, large quantities of purified protein need to be produced. This chapter describes the expression and purification of α-synuclein necessary for subsequent experiments.

3.1.1 Expression of α-synuclein in *E. coli*

An *E. coli* strain carrying a pT7-7 vector containing the SNCA gene encoding human α-synuclein 1-140 (Hoyer et al. 2004) was kindly provided by AG Hoyer from our Institute. Success of expression was controlled by SDS-PAGE followed by western blot analysis (Chapter 2.6, page 18). The blot shows a bacterial culture sample, both before and after induction of the expression of α-synuclein (Figure 7). In both cases equal amounts of cells were applied, measured by the optical density of the sample.

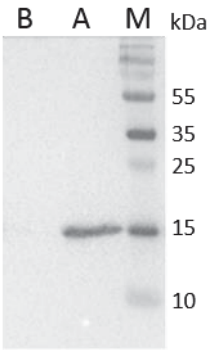

Figure 7: Western blot showing the induction of α-synuclein expression

B: Sample before induction. A: Sample after induction M: Marker (PageRuler Plus Prestained, Fisher Scientific GmbH, Germany). Primary antibody: 211 (Table 2, page 15)

While the sample before induction shows no signal, a single band of protein reactive to antibody 211 can be seen at a position corresponding to a molecular mass of ≈15 kDa.

3.1.2 Purification of α-synuclein

Following the successful expression, the protein was purified using thermal denaturation, ammonium sulphate precipitation, IEC and SEC (Chapter 2.3, page 16).

Samples from the individual steps of the purification were applied at equivalent volumes and evaluated by SDS-PAGE and Coomassie Brilliant Blue staining (Chapter 2.6 page 18).

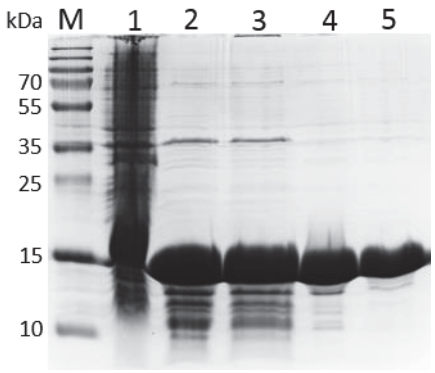

Figure 8: SDS-PAGE of the purification process of α-synuclein, stained with Coomassie Brilliant Blue

M: Marker (PageRuler Plus Prestained, Fisher Scientific GmbH, Germany), 1: Sample after cell lysis, 2: sample after thermal denaturation, 3: Sample after ammonium sulphate precipitation, 4: Sample after IEC, 5: Sample after SEC.

Figure 8 shows samples taken during the purification process. Directly after cell lysis (Lane 1), a broad smear of protein is seen in the whole lane. After thermal denaturation (Lane 2), most of this protein has disappeared but a strongly stained band of protein remains at a height corresponding to a molecular weight of ≈15 kDa. Below this band, several smaller bands remain, and two new ones appear at the very end of the lane, close to the 10 kDa band of the marker. There are also several faint bands above 15 kDa, most noticeably at 35 kDa and 70 kDa. Lane 3, containing a sample taken after ammonium sulphate precipitation, looks almost identical to lane 2, with the exception that some of the bands between 15-10 kDa are stained weaker. These bands are even less visible after the IEC (Lane 4). The bands above 15 kDa have nearly disappeared here. The sample in lane 5, after the last step of the purification, shows only a strong band at 15 kDa and two very lightly stained bands directly below it. This sample was also used for a western blot (Chapter 2.6.3, page 19), shown in Figure 9.

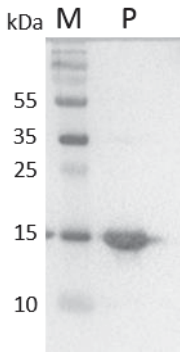

Figure 9: Western blot of purified α-synuclein.

Western blot following SDS-PAGE of α-synuclein after completed purification. M: Marker (PageRuler Plus Prestained, Fisher Scientific GmbH, Germany), P: Purified α-synuclein. Primary antibody: 211 (Table 2, page 15).

The staining shows a single band of protein bound by antibody 211 at a height corresponding to a molecular weight of 15 kDa.

The chromatogram obtained from IEC (Chapter 2.3.4, page 17) shows three peaks during the run (Figure 10).The first increase in absorption at 275 nm appears at a volume of ≈4 mL and reaches a maximum at 9 mL. After a slight decrease, the absorption increases again from 17 mL to 18 nm and then gradually decreases until 47 mL. From there it drops rapidly, until it stabilized close to zero at ≈55 mL, before the NaCl gradient starts. This is the flow through, containing material that was not bound to the column. Beginning at ≈67 mL, with the onset of the gradient, absorption increases again until it reaches a plateau, lasting from 105 mL to 115 mL. After this, the signal steadily declines until a minimum is reached at 146 mL. Here the signal increases again, and forms another plateau lasting from 167 mL to 176 mL. The chromatogram for 254 nm is in general identical to the chromatogram for 275 nm, with the difference that absorption is higher. The second and third plateau appear slightly broader, lasting from 95 mL to 123 mL and from 164 mL to 183 mL respectively.

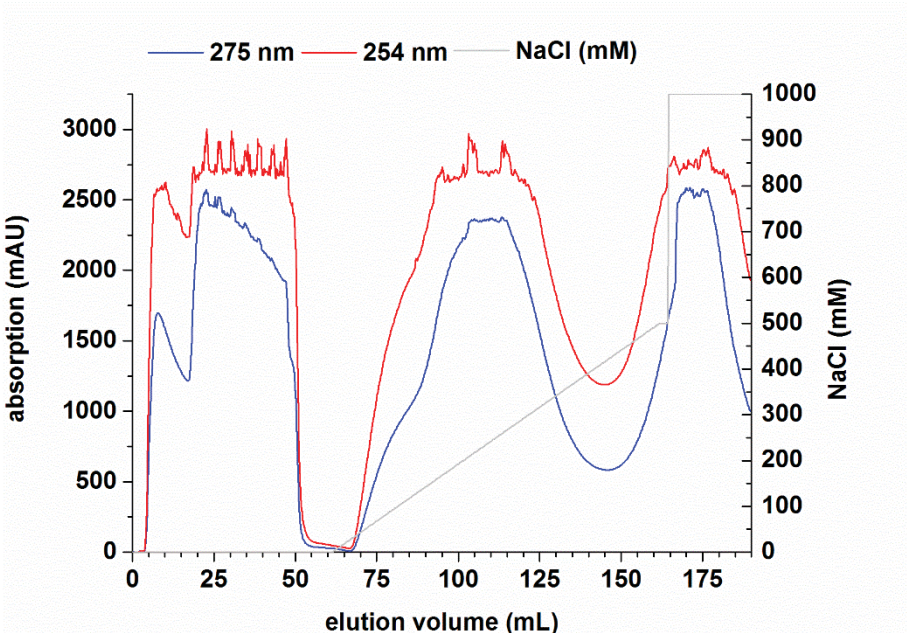

Figure 10: Ion exchange chromatography during α-synuclein purification

Shown is the absorption in mAU (left scale, red: 254 nm; blue: 275 nm) and the NaCl gradient in mM (right scale, light grey) in dependence of elution volume in mL.

The chromatogram from the SEC (Chapter 2.3.5, page 17) shows three peaks at a wavelength of 275 nm at 8, 10-12 and 15-20 mL (Figure 11). The first peak corresponds to the void volume of the column, representing molecules that were too large to be separated. The second peak is constituted of proteins with an apparent molecular weight of ≈43 kDa. The third peak represents small molecules eluted at the end of the run. The chromatogram for 254 nm shows peaks at the same elution volumes as the chromatogram for 275 nm. The first peak at the void volume of the column as well as the last peak at the end of the run show a higher absorption at 254 nm. The middle peak shows a significantly lower signal intensity.

The fractions comprising the second peak were collected, pooled and the concentration was determined by absorption spectroscopy (Chapter 2.4, page 17). On average, purification from a 1 L cell culture yielded ≈15-20 mg of pure α-synuclein. The purified protein was divided into aliquots of 100 µL, frozen in liquid N_2 and stored at -80 °C.

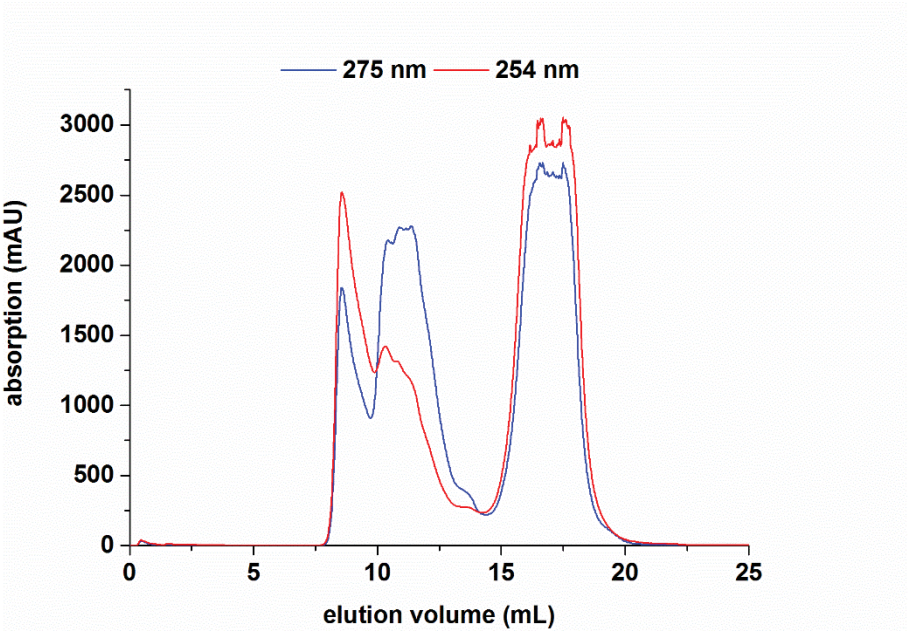

Figure 11: Chromatogram from purification of α-synuclein by SEC

Shown is the absorption in mAU (blue: 275 nm; red: 254 nm) in dependence of the elution volume in mL.

3.2 Fibrillation of α-synuclein

Fibrillation was used to provide aggregates that mimic the disease-associated form of α-synuclein found in PD and other synucleinopathies. Three different aggregation protocols were compared (Chapter 2.7, page 20). During the aggregation process, changes of the biophysical properties were monitored by CD spectroscopy and ThT fluorescence assay. In addition, the mature aggregates were visualised by AFM (Chapter 2.8, page 20). The measurements of CD spectroscopy and ThT fluorescence were partially carried out by Corvin Walter under my supervision during his work on his Bachelor thesis. The AFM measurements were carried out by Stefanie Schiefer (Institut für Physikalische Biologie, Heinrich-Heine-Universiät Düsseldorf).

3.2.1 Change in secondary structure during fibrillation

The change in the secondary structure of α-synuclein during fibrillation was measured by CD spectroscopy (Chapter 2.8.1, page 21). The resulting spectrograms are shown in Figure 12, Figure 13 and Figure 14. Figure 12 shows the change in secondary structure of α-synuclein aggregation in MES buffer over 168 h. The spectrograms show a change in secondary structure from a random coil

dominated structure at t=0 h, indicated by the minimum at 200 nm, to a β-sheet structure with a minimum at 220 nm after 48 h.

The structural change during fibrillation in Tris buffer (Figure 13) is nearly identical, also showing a random coil dominated structure at t=0 h and a β-sheet structure after 48 h. The NaP_i/SDS buffer shows a different result (Figure 14). At t=0 h, α-synuclein exists in α-helical conformation, exhibiting characteristic minima at 220 nm and 209 nm respectively. CD spectroscopy analysis indicates that within the first 24 h, complete folding into a β-sheet-dominated structure is achieved.

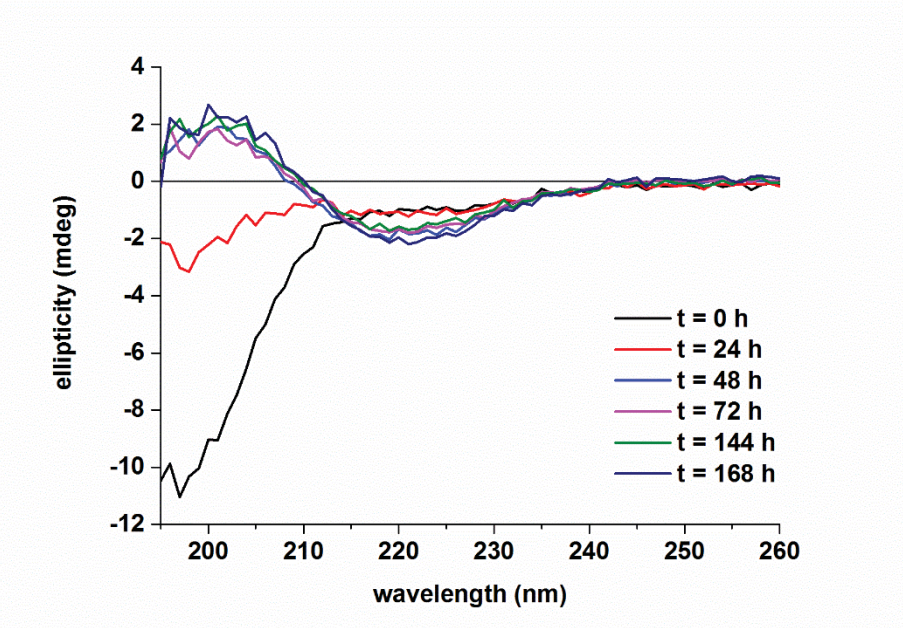

Figure 12: CD spectra of α-synuclein fibril formation in MES buffer

The spectrogram shows the ellipticity in mdeg in dependence of the wavelength in nm. Different colours indicate different time points.

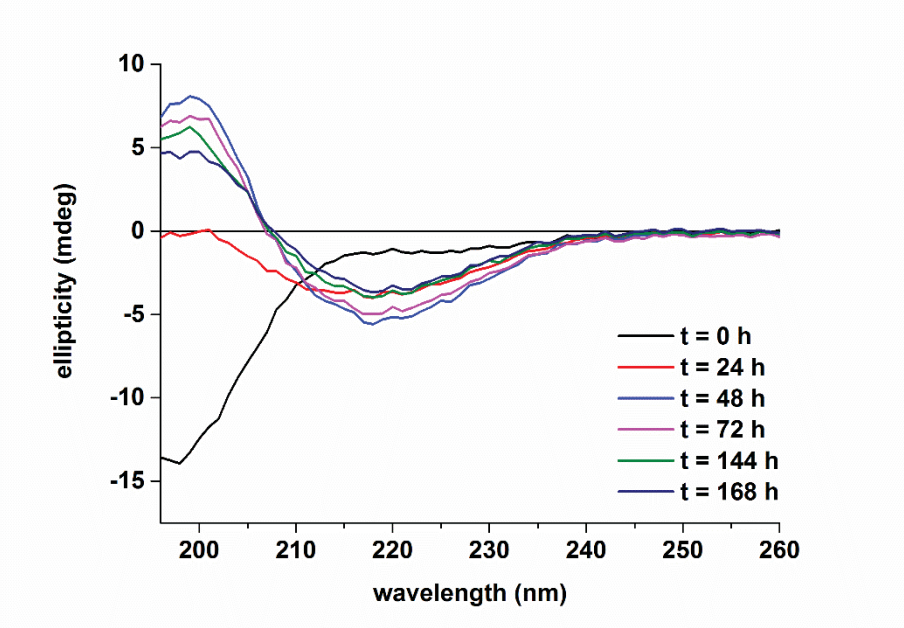

Figure 13: CD spectra of fibril formation in Tris buffer

The spectrogram shows the ellipticity in mdeg in dependence of the wavelength in nm. Different colours indicate different time points.

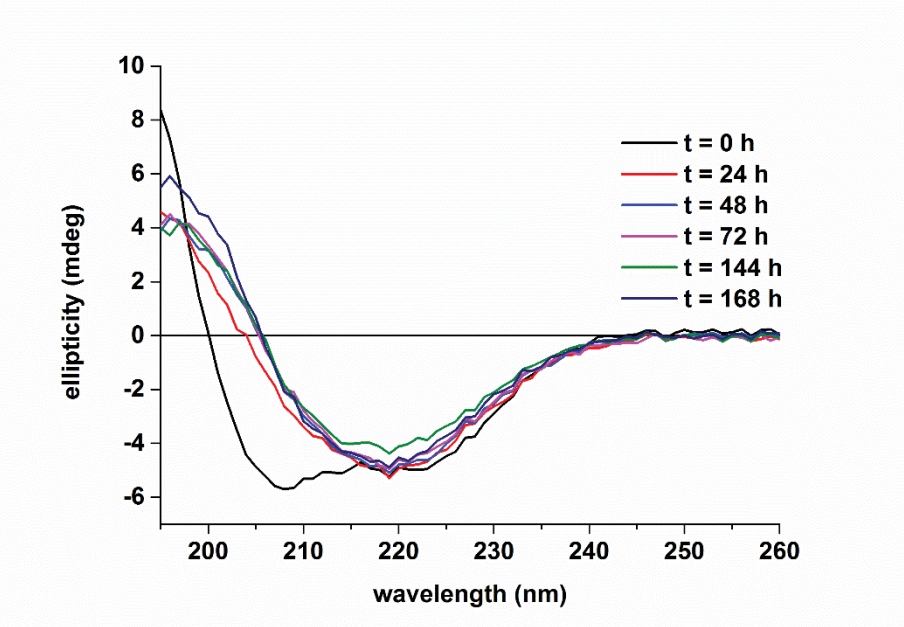

Figure 14: CD spectra of α-synuclein fibril formation in NaP_i/SDS buffer

The spectrogram shows the ellipticity in mdeg in dependence of the wavelength in nm. Different colours indicate different time points.

3.2.2 Change in ThT fluorescence during fibrillation

Formation of amyloid aggregates was investigated by ThT fluorescence assay (Chapter 2.8.2 page 21). Comparison of the time course for ThT fluorescence at 480 nm in all buffers is shown in Figure 15.

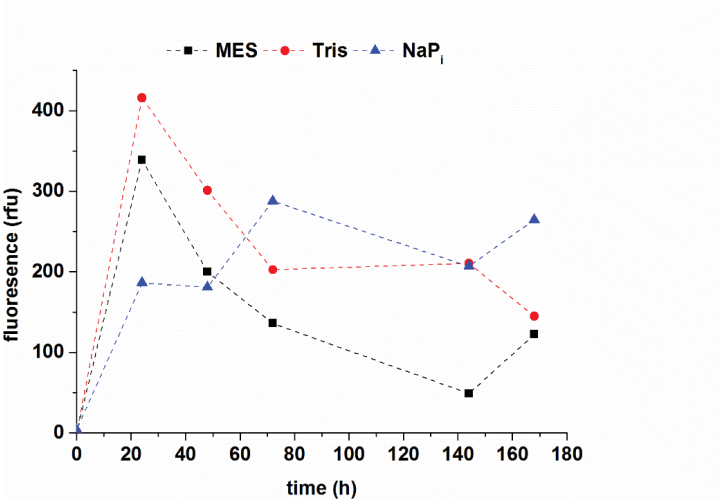

Figure 15: Amyloid fibril formation of α-synuclein in different buffers followed by increased ThT fluorescence

Fluorescence of ThT is shown at different time points for α-synuclein aggregating in MES (black square), Tris (red circle) or NaP$_i$/SDS (blue triangle).

The results for the MES buffer show an increase of fluorescence within the first 24 h. After this, the signal decreases until 144 h, and increases again slightly at 168 h. The results for the Tris buffer are very similar. Here, too, an increase is seen within 24 h followed by a continuous decrease until 168 h. The results for the NaP$_i$/SDS buffer show a maximum of fluorescence after 72 h.

3.2.3 Visualisation of aggregates by AFM

The fibrils formed by the different methods were visualised using AFM (Chapter 2.8.3).

Figure 16 shows the visualisation of fibrils formed in MES buffer.

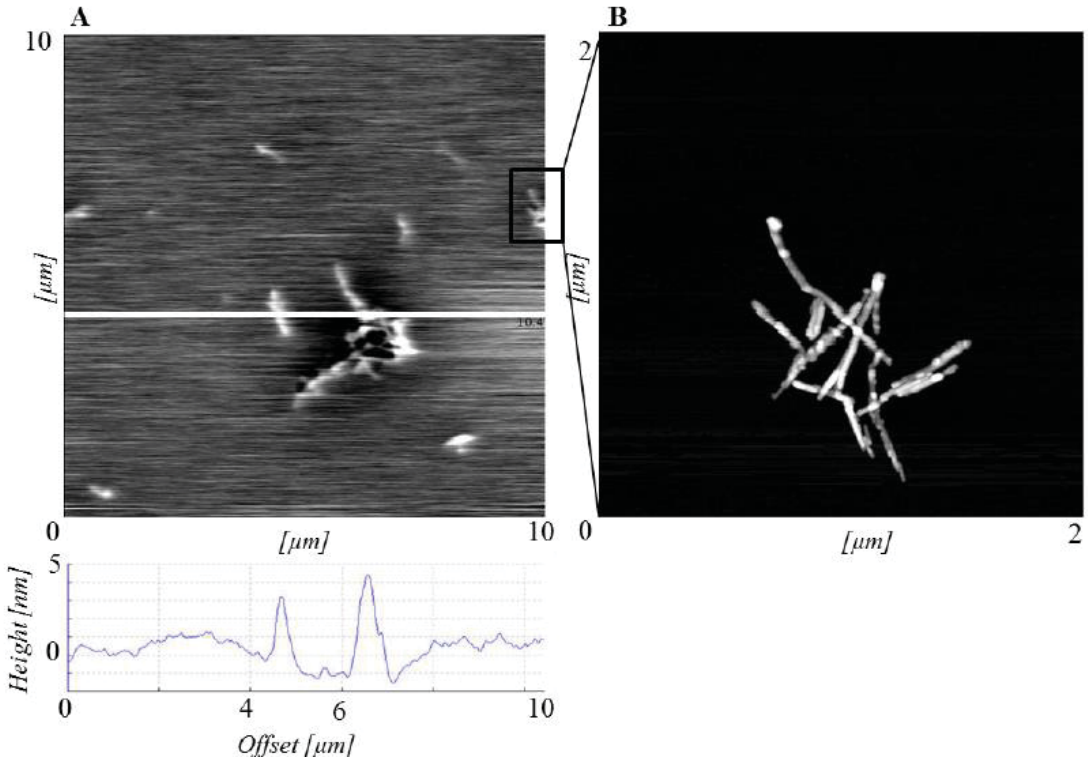

Figure 16: α-synuclein fibrils formed in MES buffer measured by AFM

A: Overview of 10x10 µm; height profile indicated by white line. B: Detailed view of a cluster of fibrils.

There are several solitary fibrils as well as clusters of fibrils visible. The height of the fibrils lies between 4-5 nm as the height profile in. Figure 16 A confirms. The length of the fibrils is in the range of several hundred nanometres.

The fibrils formed in Tris buffer are shown in Figure 17. Several single fibrils can be identified. Their length ranges from several hundred nanometres into the low micrometre scale, while their height varies between four to eight nanometres.

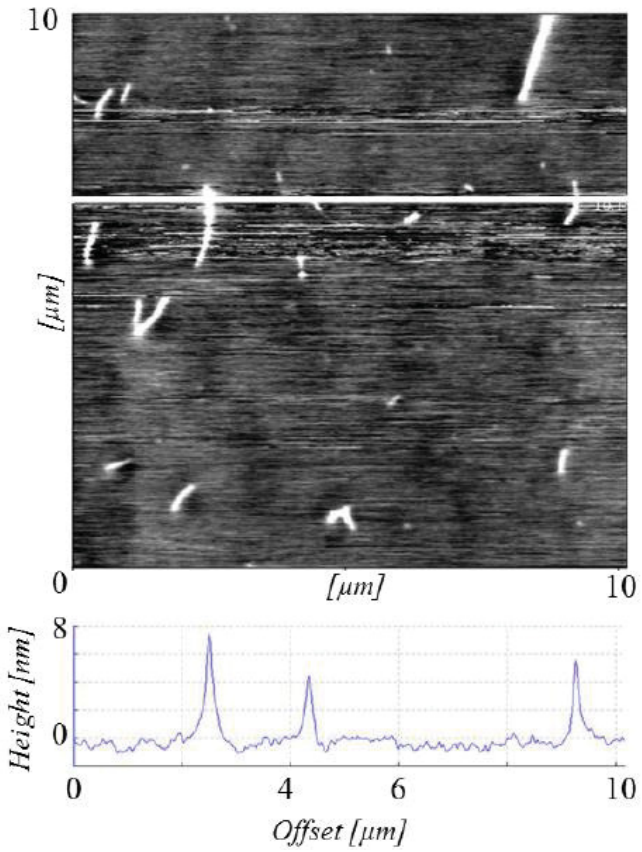

Figure 17: α-synuclein fibrils formed in Tris buffer measured by AFM

Overview of 10x10 µm; height profile indicated by white line.

The fibrils formed in NaP_i/SDS buffer are shown in Figure 18. A large number of straight fibrils can be seen, with lengths ranging from several hundred nanometres to ≈2 µm. The height ranges from 6 to 12 nm.

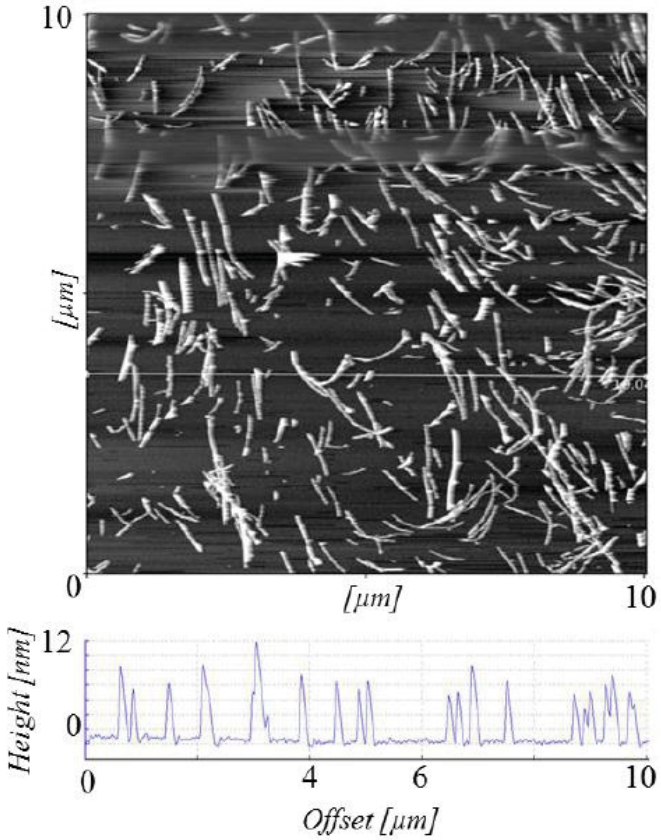

Figure 18: α-synuclein fibrils formed in NaP_i/SDS buffer measure by AFM

Overview of 10x10 µM. Height profile indicated by white line.

3.2.4 Suitability of different fibrils for sFIDA

Additionally to the biophysical characterisation of the fibrils, it is important to test them directly in sFIDA measurements. Therefore, serial dilutions of fibrils from all three buffers were prepared and measured on the CLSM according to the sFIDA protocol (Chapter 2.10).

Figure 19 shows dilutions by the factor of ten for each of the three kinds of fibrils, ranging from 10 ng to 10 pg protein per well. The samples were diluted in the respective buffer. A negative control containing no α-synuclein was measured for each buffer. The results show a fibril quantity-dependent decrease in signal strength for all three dilution series. In each case, the lowest concentration of 10 pg protein per well is distinguishable from the negative control. The sample from the NaP_i/SDS buffer shows the highest signal for each step in the dilution series and simultaneously the lowest signal for the negative control. The sample from the Tris buffer is comparable in signal strength to the sample from the MES buffer, except for the lowest concentration, where it shows a signal of about one order of magnitude greater than the respective

MES sample. The negative control for Tris is higher than that for NaP_i/SDS, but still lower that for MES.

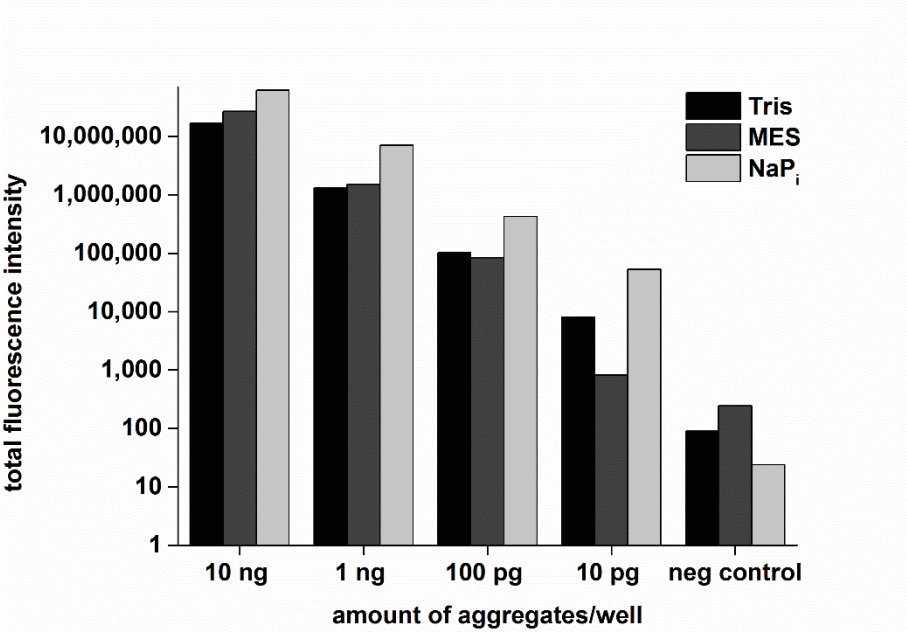

Figure 19: sFIDA shows correlation between signal strength and amount of aggregates matured and diluted in different buffers

α-synuclein fibrils were immobilized at indicated amounts and imaged by CSLM. Capture antibody: 211 Detection antibodies: 211-Alexa Fluor 488; 3H2897-Alexa Fluor 633.

To simulate the detection of α-synuclein aggregates in CSF, another dilution series was prepared, where fibrils formed in the different buffers were spiked into human CSF from healthy subjects. The samples in this serial dilution also show a decrease of signal strength with decreasing protein quantity. Fibrils formed in the NaP_i/SDS buffer exhibit the strongest signal again, followed by those formed in Tris buffer, while those formed in MES show the least signal. The difference between the signal for 10 pg protein and the negative control is lower than in the last measurement but still clearly visible.

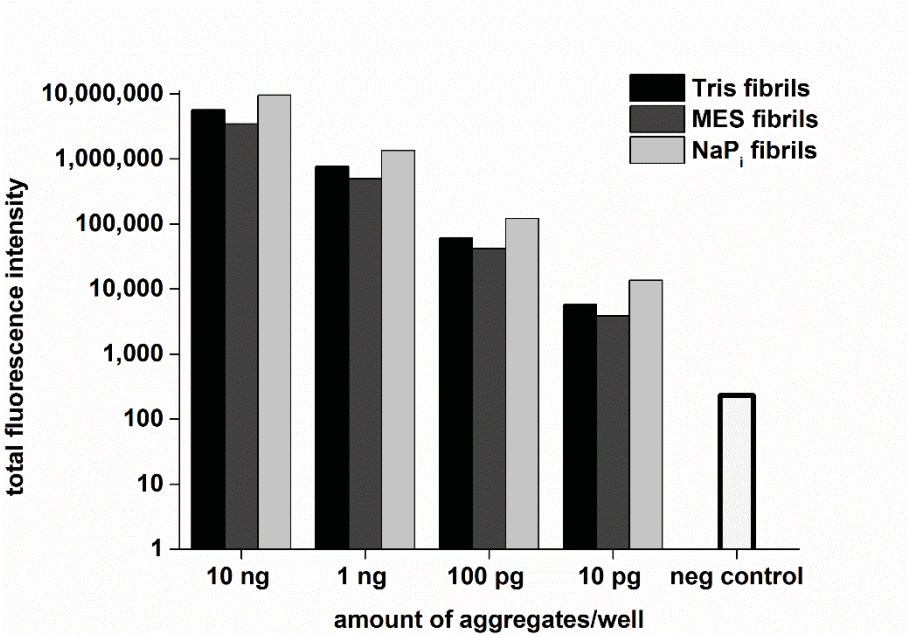

Figure 20: sFIDA shows correlation between singal strenght and amount of fibrils matured in different buffers diluted in human CSF

α-synuclein fibrils were immobilized at indicated amounts and imaged by CSLM. Capture antibody: 211 Detection antibodies: 211-Alexa Fluor 488; 3H2897-Alexa Fluor 633.

3.3 Storage of fibrils

The fibrils need to be stored for longer periods of time with minimal damage, loss or change in structure. Therefore, several storage conditions were tested and compared. The first method was to simply store the fibrils in buffer at 4 °C. This has the slight advantage that the fibrils are readily available at any time without the need for thawing or dissolving. Nevertheless, it is not suitable for long time storage, because degradation, structural changes or microbial contamination may occur more easily. The second option is to store the fibrils in buffer, but frozen at -80 °C. The storage of frozen solutions generally provides protection from microbial growth and from degradation or structural changes with time. However, the freezing and/or the thawing may prove detrimental for the fibrils. Lastly, the lyophilisation of fibrils has to be considered. Lyophilisation is the preferred method for long time storage of proteins, but the lyophilisation itself as well as the solubilisation may influence the aggregates adversely.

To find optimal storage conditions for mature fibrils, 1.4 mL of α-synuclein were fibrillated in NaP_i/SDS buffer (Chapter 2.7, page 20). The sample was then split equally into three aliquots. One aliquot was stored at 4 °C, one was frozen in liquid N_2 and stored at -80 °C, and the third was

lyophilised and stored at -80 °C. After 24 h, the frozen sample was thawed at room temperature while the lyophilized sample was solubilised in H_2O.

Concentration of soluble protein was determined in the samples and they were analysed by CD spectroscopy and AFM. The results for the different storage conditions were compared to the results of freshly prepared fibrils solution.

3.3.1 Change in fibril concentration depending on storage conditions

The total concentration of monomeric α-synuclein within the samples is 70 µM in the beginning, but it is not clear how much of this protein is finally found within the fibrils, and how much remains soluble. The amount of α-synuclein bound in fibrils was determined indirectly, by sedimentation of fibrils through centrifugation and measurement of the remaining concentration of soluble protein (Chapter 2.5, page 18). Concentration was determined directly after fibrillation for 48 h and again after 24 h of storage. The results are summarised in Table 9.

Table 9: Concentration of soluble α-synuclein depending on storage conditions

	Soluble α-synuclein	**Percentage of α-synuclein bound in fibrils**
No storage	15 µM	78,6 %
Storage at 4 °C	48 µM	31,4 %
Storage at -80 °C	32 µM	54,3 %
Storage lyophilised	60 µM	14,3 %

Concentration of soluble α-synuclein is lowest for the freshly prepared sample (15 µM). It increases by a factor of three when stored at 4 °C, by a factor of two when stored at -80 °C and it quadruples after lyophilisation.

3.3.2 AFM measurements of fibrils after storage

Storing the fibrils could potentially alter their structure or lead to the formation of non-fibrillar aggregates. To examine if the structure of α-synuclein fibrils is changed upon storage, the samples were visualised by AFM (Chapter 2.8.3, page 22).

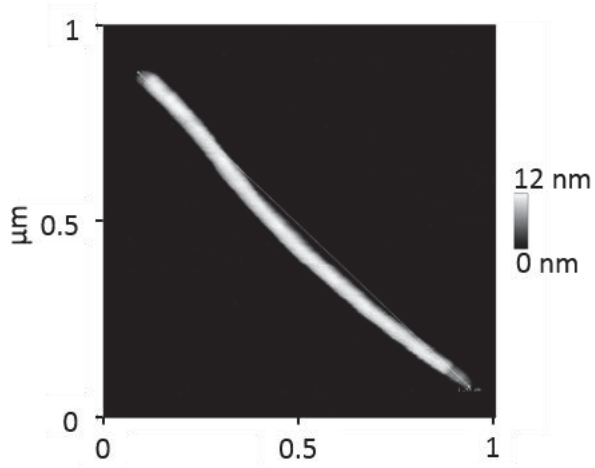

Figure 21: α-synuclein fibril imaged by AFM before storage

Example of a fibril before storage. Length: ≈1 µm; Thickness: 12 nm.

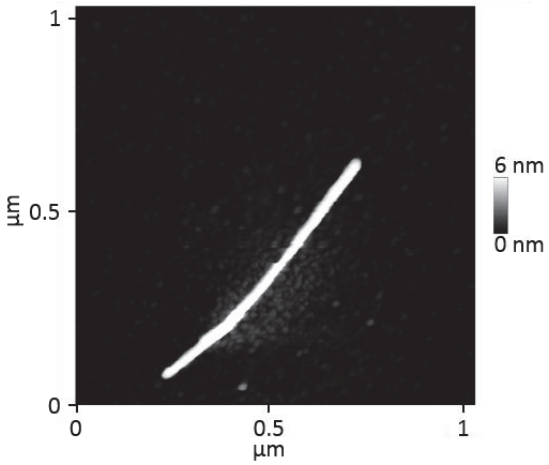

Figure 22: α-synuclein fibril imaged by AFM after storage at 4 °C

Example of a fibril after storage at 4 °C for 24 h. Length: ≈750 nm; Thickness: 6 nm.

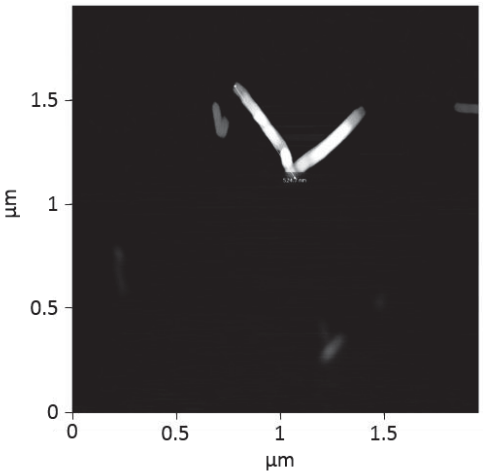

Figure 23: α-synuclein fibrils imaged by AFM after storage at -80 °C

Example of a fibril after freezing in liquid N2 and storage at -80 °C. Length: 500 nm; Thickness: 8 nm.

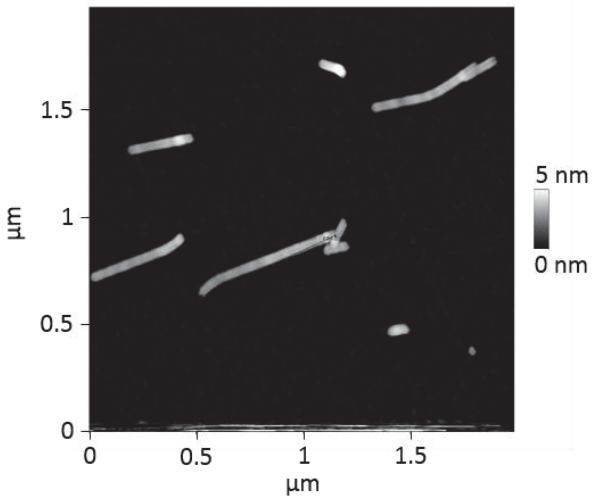

Figure 24: α-synuclein fibrils imaged by AFM after storage at -80 °C in lyophilised form

Example of fibrils after lyophilisation, storage at -80 °C and solubilisation in H_2O. Length: several hundred nanometres; Thickness: ≈5 nm.

All storage conditions cause a shortening of fibrils from 1 µm to several hundred nanometres. Fibrils also appear only about half as thick as before storage. Nevertheless, in all storage conditions fibrillar structure of α-synuclein was retained. All images show relatively straight, unbranched and untwisted fibrils and no large, amorphous aggregates appear after storage

3.3.3 sFIDA measurements of fibrils after storage

To determine whether storage conditions influence the results of the sFIDA measurements, samples obtained upon storage of α-synuclein fibrils under different conditions were measured by CLSM (Chapter 2.10.3, page 30). Samples containing 100 ng of fibrils were measured in duplicates and a well containing buffer was used as a negative control. The results are shown in Figure 25.

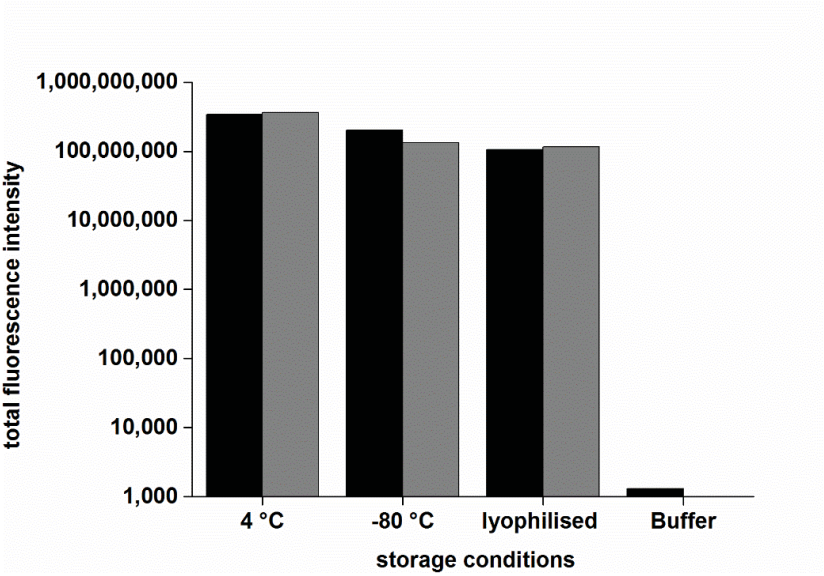

Figure 25: sFIDA of fibrils stored under different conditions shows slight loss of intensity depending on storage conditions

100 ng of α-synuclein fibrils were immobilized and imaged by CSLM. Capture antibody: 211 Detection antibodies: 211-Alexa Fluor 488; 3H2897-Alexa Fluor 633.

The signal differs only slightly both within and between the samples. Storing the fibrils at 4 °C yields the highest signal, followed by storing them in buffer at -80 °C. The lyophilised sample gives the lowest signal. All of the samples are about five orders of magnitude greater than the background fluorescence.

3.4 Preparation of fluorescently labelled antibodies

To realise the detection of α-synuclein in fluorescence microscopy, antibodies 211 and 3H2897 were labelled with the fluorescent dyes Alexa Fluor 488 and Alexa Fluor 633 (Chapter 2.9, page 22). The success and degree of labelling were confirmed through absorption spectroscopy according to the manual of the labelling kit (Data not shown).

3.4.1 SPR measurements of labelled antibodies

The affinity of the antibodies 211 and 3H2897 before and after labelling was compared using SPR (Chapter 2.9.3, page 23) to test for possible impairment of binding capabilities caused by labelling.

Each antibody was prepared in five different concentrations. The highest concentration was measured twice. Figure 26 shows that for all antibodies, independent of labelling, the response is concentration dependent. Both curves for the highest concentration are so similar in each case that they are superimposed and appear as one curve. The first 180 s show a slow, but steady association of antibodies to fibrils. From 180 s to 600 s, dissociation occurs, but at a minimal rate. The data was fitted with a 1:1 Langmuir binding model.

The data from Figure 26A+B was used to calculate the binding affinity of antibody 211 to the fibrils (Table 10).

Table 10: Kinetic parameters of the binding of antibody 211 to α-synuclein fibrils

Antibody	k_{a1}**(1/Ms)**	k_{d1} **(1/s)**	K_d
211	1,616E+6	3,387E-4	2,096E-10
211-Alexa Fluor 633	9,244E+5	7,793E-4	8,430E-10

These parameters could not be calculated for antibody 3H2897 because the association and dissociation rates were too slow, however the binding curves were comparable for both labelled and unlabelled antibody.

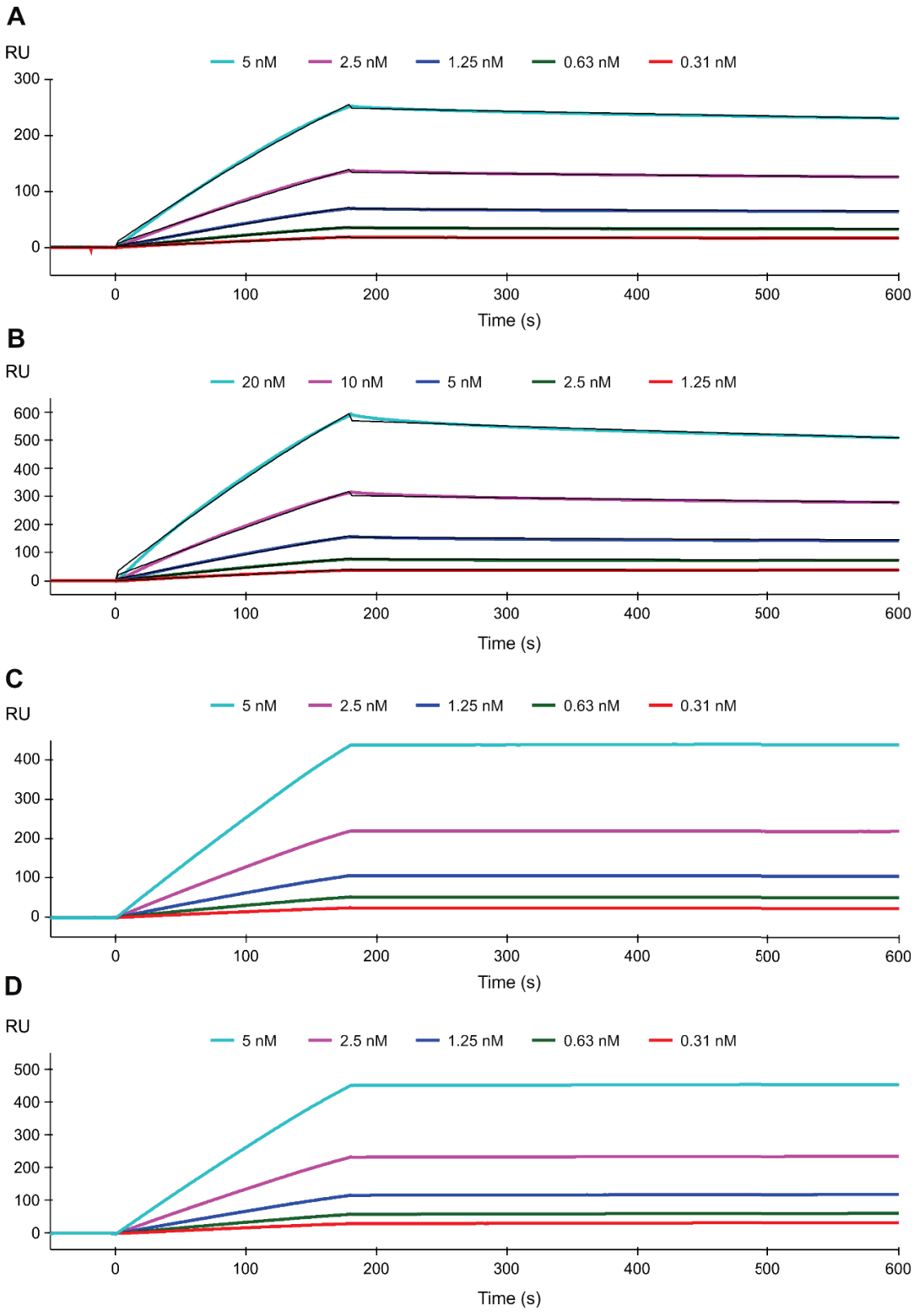

Figure 26: SPR measurements of labelled and unlabelled antibodies

The sensorgrams show the binding of antibodies to α-synuclein fibrils in resonance units as a function of time. The different colours indicate different antibody concentrations, the black lines show a fit to 1:1 Langmuir binding model. A: Binding of unlabelled antibody 211 B: Binding of antibody 211-Alexa Fluor 633 C: Binding of unlabelled antibody 3H2897 D: Binding of antibody 3H2897-Alexa Fluor 488.

3.5 sFIDA establishment

3.5.1 Comparing different antibody combinations

In chapter 3.4 it is shown that the antibodies 211 and 3H2897 are binding to α-synuclein fibrils, both before and after labelling with fluorescent dyes. To optimise the sFIDA assay, the best combination of these antibodies must be identified. Therefore, all four possible combinations were tested with a serial dilution of fibrils from recombinant α-synuclein formed in NaP_i/SDS buffer (Chapter 2.7, page 20). Fibril concentration was determined after separation from monomeric protein (Chapter 2.5, page 18) and the analysis was performed for a serial dilution ranging from 100 pg to 0.1 pg. A well containing no target protein served as a control. The results can be seen in Figure 27. For each combination of antibodies, the results for the single channels as well as for the colocalised images are given.

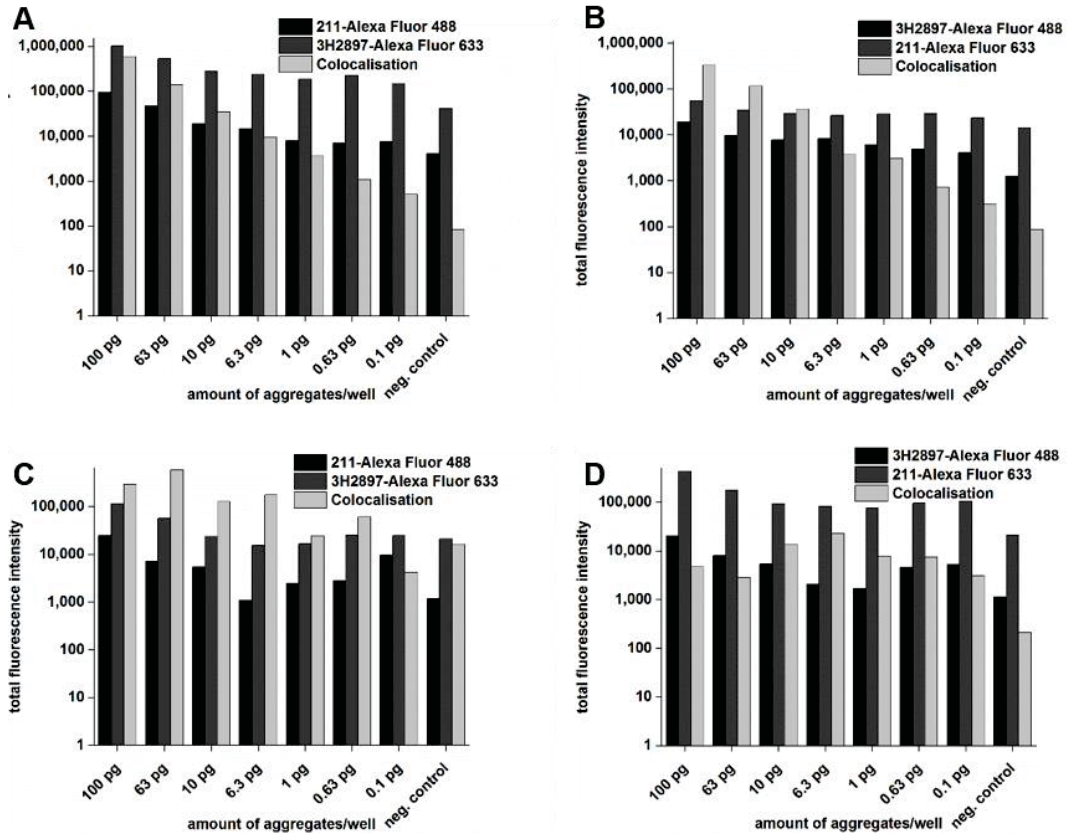

Figure 27: Comparison of sFIDA signal from different antibody combinations

sFIDA carried out with four antibody combinations, imaged by CLSM. A+B: Capture antibody 211; C+D: Capture antibody 3H2897. Black columns: Channel 1 (488); Dark grey columns: Channel 2 (633); Light grey bars: Colocalisation.

In Figure 27A, antibody 211 was used as the capture, while 211-Alexa Fluor 488 and 3H2897-Alexa Fluor 633 were used as detection antibodies. Channel1 shows a decrease in signal for the samples from 100 pg to 1 pg. For 0.63 ng and 0.1 ng there is no further decrease, but the negative control is slightly lower in intensity. The signal in Channel2 is generally higher than the signal in Channel1, but stagnates already at 10 pg, again with a lower signal for the negative control. The colocalisation of the images however reveals a different progression of the signal. Here, a constant quantity-dependent decrease of signal is discernible over all samples, with 0.1 pg still being distinguishable from the negative control.

When 211 is used as the capture with 3H2897-Alexa Fluor 633 and 211-Alexa Fluor 488 as detection antibodies (Figure 27B), Channel1 shows a slight decrease in fluorescence intensity with decreasing protein content of the samples. Only the sample containing 6.3 pg of protein breaks this trend, as it results in a minimally higher signal than the sample containing 10 pg. In Channel2, the signal decreases only from 100 pg to 10 pg, lower protein quantities show a comparable intensity. Similar to Figure 27A, the colocalisation of both channels reveals a dependency of the signal over the whole range of protein quantities, with all sample showing a signal above the negative control.

Using 3H2897 as the capture antibody leads to very different results, independent of the combination of detection antibodies. In both cases, the signals in the single channels shows no correlation between the protein content and the signal strength. The colocalisation does not improve these results.

For an easier comparison, the results for the colocalised images of the different antibody combinations were combined in Figure 28.

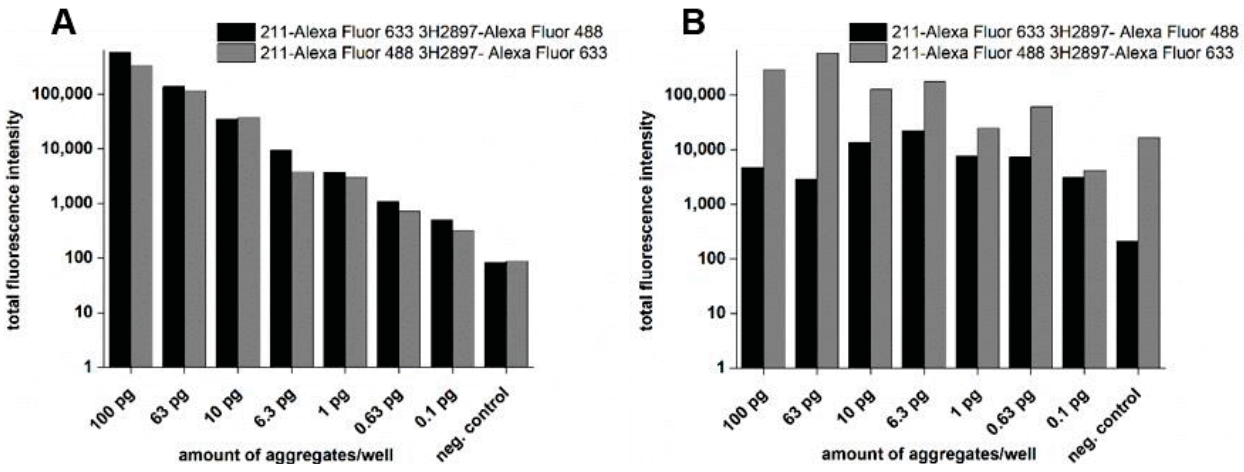

Figure 28: Influence of different capture antibodies on sFIDA

Colocalisation shows that signal strength is only correlated with amount of protein if antibody 211 is used as capture. A: Capture antibody 211; B: Capture antibody 3H2897; Black columns: Channel 1 (488); Grey columns: Channel 2 (633).

The results show that the signal strength decreases according to the protein concentration when antibody 211 is used as capture antibody (Figure 28A). Using antibody 211 labelled with Alexa Fluor 633 and antibody 3H2897 labelled with Alexa Fluor 488 shows slightly higher signals than the opposing combination, especially for the lower concentrations. When antibody 3H2897 is used as the capture, no correlation between the amount of protein and the signal strength occurs (Figure 28).

3.5.2 Validation of sFIDA measurements in buffer and CSF

Following identification of the optimal antibody combination (Chapter 3.5.1, page 56), samples containing α-synuclein monomer or fibrils, diluted in CSF of healthy subjects, were analysed by sFIDA to simulate a realistic background.

A multiwell plate was prepared according to (Chapter 2.10.1 page 25). The α-synuclein fibrils generated in NaP_i/SDS were diluted in buffer or human CSF while the monomeric α-synuclein was diluted in NaP_i/SDS. In each step, the sample was diluted by a factor of √10. Fibril concentration was determined after separation from monomeric protein (Chapter 2.5, page 18). The results for the measurement using CLSM and TIRFM are shown in Figure 29 and Figure 30 respectively.

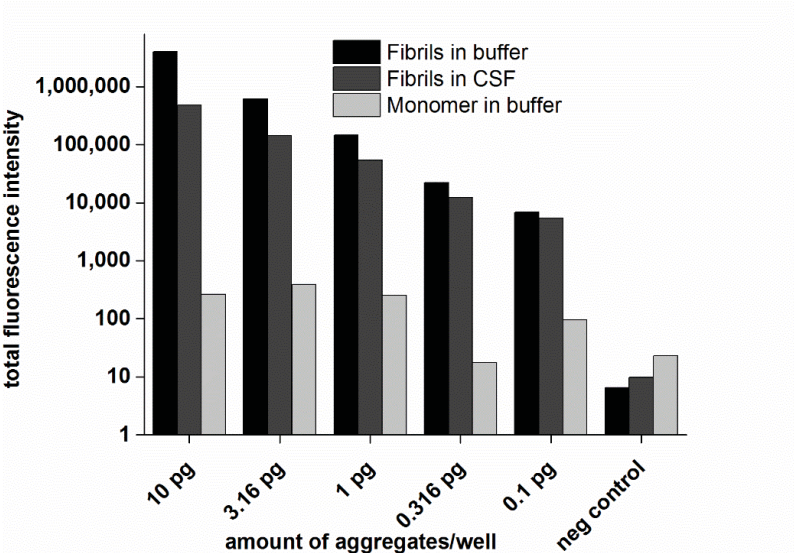

Figure 29: sFIDA is not impaired by CSF or monomeric α-synuclein

α-synuclein fibrils were immobilized at indicated amounts and imaged by CSLM. Capture antibody: 211 Detection antibodies: 211-Alexa Fluor 633; 3H2897-Alexa Fluor 488.

This sFIDA measurement using the LSM shows clearly that a decrease in fibril content results in a lowering of signal, while no such correlation can be seen for the monomer samples. The readout of the spiked CSF samples is lower than that of the fibrils diluted in buffer, while the negative control is higher at the same time. Nevertheless, in both cases the lowest amount of protein, 0.1 pg per well, still gives a noticeably higher signal than the respective negative control.

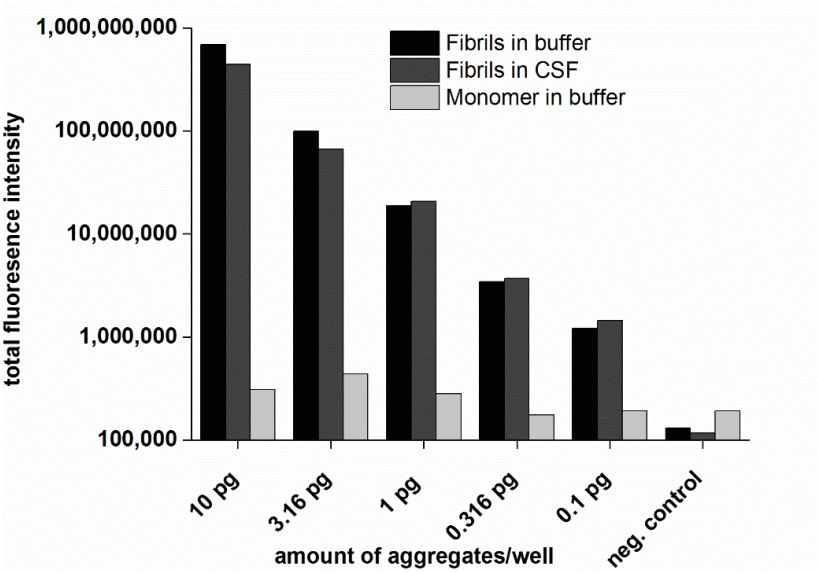

Figure 30: Influence of CSF and monomeric α-synuclein on sFIDA measured by TIRFM

α-synuclein fibrils were immobilized at indicated amounts and imaged by TIRFM. Capture antibody: 211 Detection antibodies: 211-Alexa Fluor 633; 3H2897-Alexa Fluor 488.

The results for the sFIDA measurement using the TIRF microscope match those from the LSM measurement. The samples containing monomers show no correlation between signal strength and protein content as well, while this correlation is clearly visible for the fibril samples. Spiked CSF produces slightly lower signal, but the signal to noise ratio is slightly worse when compared to the fibrils diluted in buffer.

3.6 Analysis of CSF from patients with synucleinopathies by sFIDA

In the previous chapter, sFIDA was optimised for the detection of α-synuclein by using aggregates of human recombinant α-synuclein. These aggregates serve as a model for disease associated, aggregated forms of α-synuclein which are found in several synucleinopathies.

In this chapter, CSF samples from patients with either MSA or PD were analysed and compared to CSF from healthy subjects.

3.6.1 sFIDA measurements of MSA samples

CSF samples from five patients with MSA were analysed by sFIDA. A multiwell plate was prepared using 20 µL of each samples as target (Chapter 2.10.1, page 25). Negative controls were prepared

by using CSF from healthy patients and PBS, and a positive control was prepared using 1 ng of α-synuclein fibrils. All samples were measured in triplicates and the results are shown in Figure 31.

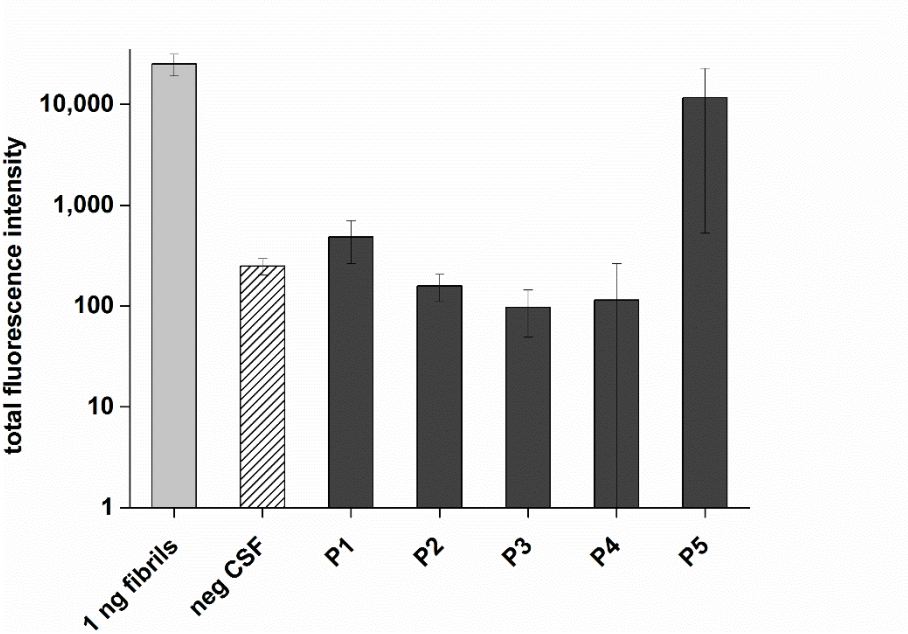

Figure 31: sFIDA of MSA samples, colocalised

Measurement of CSF from patients (P1-P5) with MSA samples (dark grey) in comparison to CSF from healthy subjects (black/white stripes) and a positive control of recombinant fibrils (light grey). Error bars show standard deviations between the samples measured in triplicates. sFIDA measured by CLSM. Capture antibody: 211; Detection antibodies: 211-Alexa Fluor 633, 3H2897-Alexa Fluor 488.

The graph shows that only the sample “PL Post M” can be distinguished from the negative controls. All other samples are overlapping with the standard deviation of the controls, or are even lower.

3.6.2 sFIDA measurements of PD samples

To test the suitability of the sFIDA for PD diagnosis, CSF samples from patients with PD were measured. A sample containing 10 ng of recombinant α-synuclein fibrils was used as a positive control, while PBS and CSF from healthy subjects were used as negative controls. The positive control was measured in triplicate to provide a plane of focus in each row of the multiwell plate. All other samples were measured in duplicates. The resulting intensity of the colocalised images are shown in Figure 32.

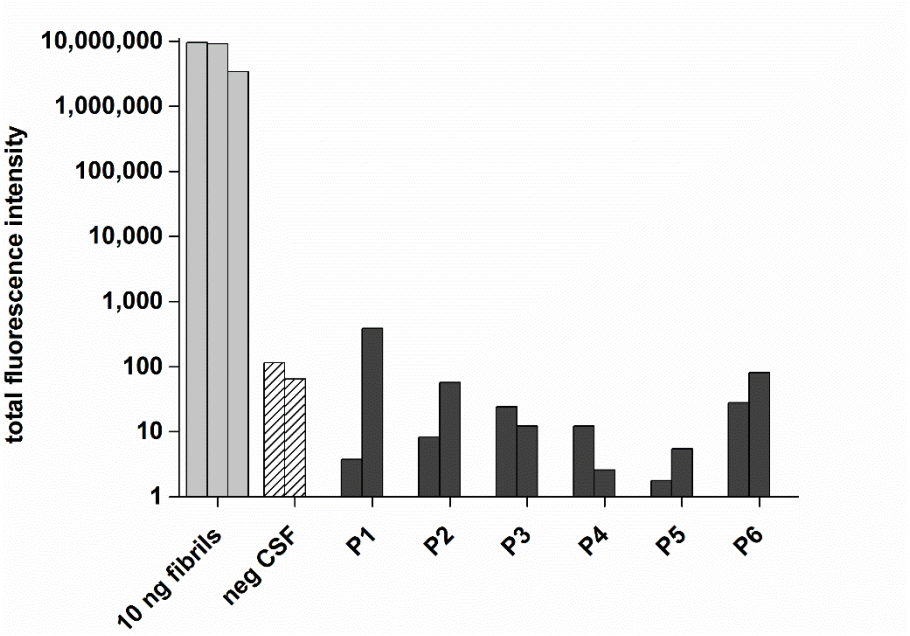

Figure 32: sFIDA of PD samples, colocalised

sFIDA of CSF samples from patients with PD, measured in duplicates (dark grey), in comparison to CSF from healthy subjects (black/white stripes) and a positive control of recombinant fibrils (light grey). The positive control was measured in triplicate to improve calculation of the focus plane for automated measurement. sFIDA measured by CLSM. Capture antibody: 211; Detection antibodies: 211-Alexa Fluor 633, 3H2897-Alexa Fluor 488.

The graph shows that samples from patients P3-P5 exhibit less signal CSF from healthy subjects. Patients P2 and P6 are at roughly the same level as the CSF from healthy subjects and cannot be clearly distinguished, while signal of CSF from patient P1 shows a higher signal in one sample and a lower signal in the duplicate.

4 Discussion

4.1 Expression and purification of α-synuclein in high yield and purity

Production of α-synuclein at high purity is necessary to provide enough protein for the subsequent experiments. Therefore, the expression of human recombinant α-synuclein in *E. coli* and its purification were established at the beginning of this study.

The appearance of signal on the western blot after induction showed that α-synuclein was expressed, confirmed both by binding of a specific antibody as well as the correct molecular weight of 15 kDa (Figure 7, page 37).

The SDS-PAGE (Figure 8, page 38) indicated that the removal of protein impurities was successful. The sample after cell lysis is stained throughout the whole lane, as all proteins the *E. coli* cells produce are still included. After the thermal denaturation and centrifugation, most of these impurities were removed, but a strong band of α-synuclein remained at ≈15 kDa. While α-synuclein is thermostable and remains soluble even under high temperatures, most other proteins denature under these conditions and become insoluble. Subsequent centrifugation separated denatured protein from soluble α.synuclein. A protein with a molecular weight of ≈35 kDa remained until it was removed during the IEC. Some bands appeared in the range of 10-15 kDa. They were gradually removed during the purification process, mainly through IEC and SEC. The western blot of the purified sample (Figure 9, page 39) confirmed that the purified protein was α-synuclein.

The chromatogram of the IEC (Figure 10, page 40) showed three sections of increased absorbance at both 254 nm and 275 nm. The first peak appeared during washing of the column with a buffer containing no NaCl and thus contained molecules that did not bind to the column under the given conditions. The second peak appeared at a concentration of ≈300 mM NaCl during the linear gradient, which is in accordance with published results for IEC of α-synuclein (Hoyer et al. 2002). It is broadened at maximal absorption, which might indicate that the column was overloaded. Absorption at 254 nm is slightly higher that the absorption at 275 nm, meaning that the peak did not contain pure protein but was contaminated, probably with nucleic acids. The last peak, appearing at the end of the gradient at high concentrations of NaCl contained impurities that bound very strongly to the column.

The separation of α-synuclein from proteins included in two other peaks clearly showed the purification effect achieved by IEC. Both peaks had a higher absorbance at 254 nm, indicating that

they are not comprised purely of protein, but do include nucleic acids. Since nucleic acids are not detected by the Coomassie staining their removal cannot be followed by the SDS-PAGE.

The SEC chromatogram (Figure 11, page 41) showed three different peaks. First a sharp, distinct peak appeared at 8 mL, the void volume of the column. This peak showed a higher absorption at 254 nm than at 275 nm, indicating that it contained mostly nucleic acids. The second peak at 10-12 mL, containing α-synuclein, is characterised by a higher absorption at 275 nm, meaning that nucleic acid impurities were removed. Similar to the IEC, it also forms a plateau, which again might indicate overloading of the column. Since after this step α-synuclein was of high purity, the oberloading of the column did not affect the purity of the eluted sample. The third peak eluted at the end of the run and contained molecules that are too small to be separated by the column. The separation of the middle peak from the other two showed that the SEC contributes to purifying the protein further. Moreover, since the absorbance at 254 nm is significantly lower than at 275 nm the protein seems to be no longer contaminated with nucleic acids.

The preparation of α-synuclein from a 1 L *E. coli* cell culture yielded ≈15 mg of pure protein.

Overall, the purification method used in this study was effective, yielding high amounts of monomeric α-synuclein with high purity.

4.2 Fibrillation of α-synuclein and comparison of different buffer systems

Monomeric α-synuclein was successfully expressed and purified, as described in chapter 3.1. To develop the sFIDA assay, a-synuclein aggregates were required. Therefore, in the next step optimal conditions for fibrillation of α-synuclein were established. For this purpose, three different conditions during aggregation of a-synuclein were tested. Aggregation was tested at pH 7.7 in Tris buffer and compared to aggregation in more acidic conditions (MES buffer pH 6.0) as well as to aggregation in presence of SDS (NaP_i pH 7.7, 0.5 mM SDS). SDS is reported to increase rate of aggregation as well as reproducibility (Giehm et al. 2011). The changes in secondary structure and the occurrence of amyloid aggregates were monitored throughout the fibrillation process. After fibrillation was accomplished, AFM images were taken to visualise the resulting fibrils.

4.2.1 Change in secondary structure occurs fastest in NaP_i/SDS buffer

α-synuclein is a natively unfolded protein, showing no secondary structure in solution (Weinreb et al. 1996). Fibrils on the other hand are defined by a cross-β structure (Sawaya et al. 2007). This conformational change can be observed using CD spectroscopy (Chapter 2.8.1, page 21) to monitor the formation of fibrils.

A change from a random-coil dominated spectrum exhibiting a minimum at 200 nm to a spectrum typical of β-sheet structure, characterised by a maximum at 195 nm and a minimum at 215 nm, was observed for the sample in MES buffer within 48 h (Figure 12, page 42). Similarly, the sample in Tris buffer (Figure 13, page 43) underwent structural changes from a random-coil to a β-sheet dominated structure within the same timeframe, but continued to show minor changes even after 168 h. α-synuclein dissolved in the NaP_i/SDS buffer featured minima at 209 nm and 220 nm characteristic for α-helical secondary structure (Figure 14, page 43). Formation of an amphipathic α-helix has been previously observed for α-synuclein and this effect has been ascribed to the interaction of the protein with SDS (Giehm et al. 2010). The change into a β-sheet structure is completed within 48 h.

In MES and NaP_i/SDS buffer, the change of structure into β-sheets appears at comparable rates and is finished after 48 h, but in Tris buffer it takes considerably longer, at least 168 h.

4.2.2 Formation of ThT-positive α-synuclein aggregates occurs within 24 h in all buffers

The characteristic change of the emission from the fluorescent dye ThT upon binding to amyloid aggregates was monitored to complement the results acquired through the CD spectroscopy measurements (Chapter 3.2.2, page 44). All three samples showed an increase of fluorescence intensity at 480 nm within the first 24 h. From there on, the signal generally decreases, although with some fluctuations. This is a common occurrence in ThT fluorescence measurements of fibrils, the cause of which this is not well understood. One possible explanation is that with increasing aggregate size, formerly accessible ThT binding sites are concealed as new layers of protein are added to the existing aggregate. While this might be a suitable explanation for spherical or amorphous aggregates it seems less likely in case of the uniformly shaped fibrils which continually bind monomers on their outer ends (Collins et al. 2004, Esler et al. 2000). Another possibility is that the binding of ThT to the fibrils leads to a very high local concentration of dye in proximity to the fibril. This could then cause some of the ThT molecules to be shielded by others closer to the light source and thus not being excited, resulting in decreased fluorescence. A high concentration of dye molecules might also lead to increased quenching, resulting in decreased fluorescence independent

of absorption. In addition, with growing size the fibrils might sediment to the bottom of the cuvette so that they cannot be measured by fluorescence spectroscopy anymore.

In conclusion, a specific change in the ThT fluorescence confirmed that the structural change measured by CD spectroscopy indeed represented the formation of β-sheet rich amyloid aggregates. However, this assay does not allow conclusions as to the amount of aggregates formed. A positive signal was detected after 24 h in all three samples.

4.2.3 Fibrils obtained in all buffers show similar morphology in AFM

AFM was used to visualise the samples at the end of the aggregation process. Fibrils with a length of several hundred nanometres were clearly visible in all three buffers. The difference in height ranges from 3-5 nm for fibrils formed in MES to 4-8 nm for those formed in Tris and finally to 4-12 nm for those formed in NaP_i/SDS. It is well known that the structure of the fibrils is influenced by the conditions applied during the fibrillation. Depending on pH and ion conditions, fibrils are either straight or show a twisted ribbon morphology, while acidic conditions below pH 4 lead to the formation of amorphous aggregates instead of fibrils (Heise et al. 2005, Hoyer et al. 2002). Length and thickness of the fibrils formed here is in accordance with published data (Bousset et al. 2013).

4.2.4 Fibrils formed in NaP_i/SDS are most suitable for sFIDA

The analysis of the different fibrils showed very similar results in sFIDA measurements when diluted in the respective buffer (Figure 19, page 48) or in human CSF (Figure 20, page 49). The fibrils generated in NaP_i/SDS buffer showed a slightly higher signal in both cases. Most importantly, they showed the highest signal to noise ratio when comparing the signal of the lowest quantity of α-synuclein to the respective negative control.

4.2.5 Conclusion: NaP_i/SDS buffer assures fast fibril formation and high signal intensity in sFIDA

The formation of fibrils was achieved independent of the buffer used. The occurrence of amyloid aggregates confirmed by ThT fluorescence took place equally fast independent of the buffer used. The fibril morphology observed in AFM varied only slightly and was in accordance with results published in literature (Bousset et al. 2013). Aggregates generated in all buffers clearly exhibited fibrillar structures with only minor differences in length and height. While these methods showed

a successful fibril formation, they yielded no information as to which protocol should be used to produce fibrils for the development of sFIDA.

The change in secondary structure into a stable β-sheet conformation was fastest in MES and NaP_i/SDS buffer, taking only 48 h, whereas in Tris buffer conversion was observed at 168 . The measurement by sFIDA showed both the highest signal and the highest signal to noise ratio for the NaP_i/SDS derived fibrils, indicating that fibrils formed under these conditions are more readily bound by the antibodies in sFIDA. This effect was observed for samples diluted in buffer as well as in CSF (Chapter 3.2.4, page 47). Combining these results, NaP_i/SDS was considered the most suitable buffer for fibril formation, as fibrillation was fastest and the fibrils showed the highest signal as well as signal-to-noise ratio in sFIDA measurements.

4.3 Storage of α-synuclein fibrils

4.3.1 Loss of α-synuclein fibrils is lowest if fibrils are stored in buffer at -80 °C

The concentration of α-synuclein fibrils decreases for all tested storage conditions (Table 9, page 50). Directly after aggregation, 78.6 % of the initial α-synuclein is bound in fibrils. This reduces most extremely with lyophilisation of the fibrils, after which only 14.3 % of the protein was found to be in fibrillar form. Storing the fibrils at 4 °C reduced the amount of fibrillar α-synuclein to 31.4 %. However, long-term storage of protein at 4 °C is not advised for several reasons. At this temperature, microbial growth can only be prevented by compromising the purity of the sample through addition of bacteriostatic agents like sodium azide. More importantly, changes in the structure of the fibrils might continue to take places over longer periods of time, which was not evaluated in this study. Freezing the sample in liquid N_2 and successive storage at -80 °C showed the least impact on fibril concentration, with 54.3 % of the protein content remaining in fibrillar form.

This proved that storing the fibrils at -80 °C was the most suitable method in terms of long time storage. Consequently, all fibrils were aliquoted and stored in these conditions from here on.

4.3.2 Fibril morphology is not affected by storage as analysed by AFM

AFM measurements of fibrils before and after storage revealed no major impact of storage conditions on fibril morphology. All samples showed single, straight fibrils of comparable width and height. Fibrils after lyophilisation or storage at -80 °C were both minimally shorter than freshly prepared fibrils or those stored at 4 °C, but were very similar if compared to one another. Thus, AFM analysis confirmed that storage did not influence the morphology of the fibrils irrespective of the storage conditions.

4.3.3 sFIDA reveals little difference between storing methods if equal amounts of aggregates are applied

Fibrils were used to mimic the disease form α-synuclein while establishing sFIDA, so the effect of their storage on the outcome of this method had to be tested. It is not clear if the aggregated protein can be still transferred onto the surface of the multiwell plate in sFIDA and if it is still as recognisable by the antibodies as before. Therefore, the three samples after24 h of storage were compared in sFIDA (Figure 25, page 53). The results showed that, compared to storage at 4 °C, a minor decrease of signal occurred with freezing of the sample. Lyophilisation showed a slightly greater decrease in fluorescence. All samples were clearly distinguishable from the negative control. This experiment showed that storage did not impair the detectability of α-synuclein aggregates by sFIDA if the change in concentration is compensated.

4.3.4 Conclusion: Storing fibrils in buffer at -80 °C is the preferable method, but the fibril concentration needs to be reassessed before further use

The results presented in chapter 3.3 showed that long-term storage of a-synuclein is feasible as the structure of fibrils and their detectability via sFIDA were preserved. . Comparison of different storage methods revealed that the significant factor influencing the storage is the yield of fibrils which remained in thawed sample. The lowest loss of fibrils was observed when the liquid samples were frozen at -80 °C. Based on these results, this condition was chosen as the preferable way to store α-synuclein fibrils and was subsequently used for all samples in this study. No publication detailing the storage of amyloid fibrils and its effect on concentration or structure was found to compare these data to.

Another important information derived from these experiments is that the ratio of soluble to aggregated protein changes during storage. Consequently, the actual amount of aggregated protein

must be reassessed in each sample before conducting any experiments. Without this additional control the amount of aggregated protein in the sample is not known as the conversion from aggregated to monomeric α-synuclein during storage is neglected.

Based on these results, the determination of concentration of aggregated α-synuclein (Chapter 2.5, page 18) was introduced to ensure reliability of the measurements by guaranteeing that equal quantities of α-synuclein are applied. For this purpose, the matured fibrils were separated into aliquots before freezing. For each measurement, 100 µL from one aliquot were used in the centrifugation, while the rest was stored on ice. The supernatant from the centrifugation was used to determine the amount of soluble protein in the sample, and thereby indirectly the amount of aggregated protein. All calculations concerning the amount or concentration of fibrils in this specific sample were then based on these individually determined values, and the appropriate volumes were taken out from the remaining aliquot that was not subjected to centrifugation.

4.4 SPR measurements indicate no loss of function of antibodies through labelling

Labelling can potentially alter the affinity of antibodies, as shown in a study were the affinity of an antibody for the antigen before and after labelling with 5-fluorotryptophan was compared by SPR (Acchione et al. 2012).

To elucidate if conjugation of the fluorescent dye caused a steric hindrance influencing binding affinity, the kinetic constants and the equilibrium constants for the interaction of labelled and unlabelled antibodies to α-synuclein fibrils were studied by SPR (Chapter 2.9.3, page 23).

The association and dissociation rate for labelled and unlabelled antibody 211 were very similar, meaning that the affinity of 211 to α-synuclein fibrils was not affected by the fluorescent dye (Table 10, page 54). Sensorgrams for antibody 3H2897 showed slow kinetics both for labelled and unlabelled variant (Figure 26, page 55). Since kinetic constants approached the limits that can be measured by the instrument, direct comparison of the association and dissociation rate constants for this antibody was not possible. Nevertheless, the binding of labelled and unlabelled antibodies seemed to follow similar kinetics meaning that dye incorporation did not affect the affinity as well. In both cases, the association was unusually slow for an antibody-antigen binding, showing nearly a linear progression where a fast, exponential increase in RU is expected.

The reason for the slow association and the difficulties in fitting kinetic parameters are unclear. Binding between antibodies and fibrils may be complicated by fibril structure. It is not clear how close the epitopes on the fibril surface were to each other and if both binding sites of a single antibody bound to the same fibril, to two different fibrils, or if just one site was involved in binding. Furthermore it is unknown how the fibrils are bound to the surface. Ideally they would lie parallel to the surface, but they might also partially point into the flow chamber. If part of a fibril is not in close proximity to the surface, binding of the antibody will not be detected by the instrument.

SPR measurements might be improved in several ways. Immobilisation of less fibrils could produce a more reliable signal. For measurements where the molecules bind with a high affinity, high temperature of around 37 °C are often advised to increase dissociation.

However, although the details of the binding cannot be analysed here, the similarities prior to and after labelling do confirm that binding is not compromised by labelling.

4.5 Establishing sFIDA with recombinant aggregates

4.5.1 Choice of capture antibody as well as colocalisation of images are critical for sFIDA

The test of different antibody combinations in Chapter 3.5.1 (Page 56) demonstrated two important aspects of the sFIDA method.

Firstly, the results presented in Figure 27A+B (Page 56) indicate the advantage gained by using colocalised images compared to images from single channels. While all samples resulted in a higher fluorescence than the negative control, they became indistinguishable from each other when the amount of protein reaches the low picogram range in single channel measurements. This effect is completely offset when comparing the results after colocalisation. Here, the decrease in protein content showed as a decrease in signal throughout the whole range of samples, from 100 pg to 0.1 pg, with all samples being discernible from the negative control. This increase in sensitivity occurred despite lowering of the overall signal in the colocalised images in most samples. The reason for this is that colocalisation reduces signals that are only present in one channel (Chapter 2.11.1, page 32).

Secondly, the choice and combination of different antibodies seemed to have a major impact on the results. In Figure 28 (page 56), it became evident that when using antibody 211 as capture, a

positive correlation between protein content and signal strength was achieved, while replacing the capture with antibody 3H2897 caused a loss of this correlation. Consequently, 211 was chosen as the capture antibody while 3H2897 was considered unsuitable for this purpose. The combination of the detection antibodies did not have a significant impact on the measurements. Signal strength was minimally higher with the combination 3H2897-Alexa Fluor 488/211-Alexa Fluor 633 (Figure 28: Influence of different capture antibodies on sFIDA, page 58). Therefore, the combination of these labelled antibodies and antibody 211 as capture is considered as optimal and chosen for further experiments.

4.5.2 sFIDA enables detection of α-synuclein aggregates in CSF

In chapter 4.5.1 (Page 56) the optimal parameters of the sFIDA obtained using recombinant α-synuclein fibrils diluted in buffer as target were presented. When measuring human CSF samples, two major challenges can be anticipated that were addressed in chapter 3.5.2.

The first potential problem is caused by the composition of the CSF. Unlike the solutions of purified recombinant protein, it also contains other proteins and other cellular components, like lipids, which might interfere with the measurement. Antibodies may be unable to bind due to blocked epitopes or show cross-reactivity, and autofluorescent molecules could increase background, for example.

The second possible obstacle is the content of monomeric α-synuclein in CSF samples. As α-synuclein usually exists in a monomeric state, CSF samples will probably contain monomeric α-synuclein too. This might impair measurements, for example if an excess of monomeric protein competes with aggregates for binding sites on the surface.

To simulate these conditions, fibrils diluted in buffer were compared to those diluted in CSF of a healthy subject and to monomeric α-synuclein at equal amounts. The results, measured by CLSM and TIRFM, can be seen in Figure 29 (Page 59) and Figure 30 (Page 60) respectively.

The comparison of measurements for fibrils diluted in buffer and in CSF showed that both, overall signal as well as signal-to-noise ratio, were lower for the CSF samples. Nevertheless, even the sample containing 0.1 pg of fibrils was clearly distinguished from the negative control.

Recent studies have shown the total concentration of α-synuclein in CSF from patients with PD, MSA and DLB to be 1.2-1.4 pg/µL, 0.9-1.3 pg/µL and 1.1-1.4 pg/µL, respectively (Mollenhauer et al. 2011). This indicates that sFIDA is sensitive enough to detect the quantities of α-synuclein that are to be expected in CSF samples. The amount of aggregated α-synuclein is probably considerably

lower, however larger sample volumes can easily be used. Up to 100 µL of sample can be applied to the well at one time, and it would also be possible to increase the analysed volume further by applying the sample several times to the well, accumulation α-synuclein at the surface.

The samples containing monomeric α-synuclein showed no concentration dependence and lower signal than the samples containing fibrils by at least an order of magnitude for each concentration.

According to these results, proof-of-concept was delivered that sFIDA enables detection of α-synuclein aggregates in CSF.

4.5.3 sFIDA adaption to clinical samples

After establishing of the sFIDA using recombinant protein and spiked CSF samples, the assay was tested with CSF samples from MSA patients (Chapter 3.6.1., page 60) and PD patients (Chapter 3.6.2, page 61).

The results showed that the CSF samples from MSA patients cannot be clearly distinguished under consideration of the standard deviations (Figure 31, page 61). The samples from patients P2-P4 exhibited slightly lower signals than the CSF from heathy subject, while sample P1 showed slightly higher signal. The sample collected post mortem showed a significantly higher signal than the negative control. Of the PD samples, three out of six (P3-P5) could be clearly differentiated from the control, exhibiting lower signals, whereas two others (P2-P6) were of a comparable level to the CSF sample from a healthy subject. The signal exhibited from the sample of CSF from patient 1 could not be distinguished from the control, as one measurement showed a higher signal while the duplicate showed a lower signal.

Although three out of six PD samples could be clearly differentiated from the control, several parameters need to be optimized to increase the sensitivity of the sFIDA. As the results presented in chapter 3.5.1 show, the choice of antibodies can greatly improve the correlation between the concentration of α-synuclein aggregates and the signal strength. Using antibodies recognising different α-synuclein epitopes might result in a higher specificity for α-synuclein aggregates present in clinical samples and lead to an improved signal-to-noise ratio. Conformation-specific antibodies have been found for amyloid-β (Kayed et al. 2010, Kayed et al. 2007). If such antibodies were available for α-synuclein they could greatly impact the specificity of sFIDA analysis of CSF samples.

To further optimise sFIDA in terms of improvement of signal-to- noise ratio he sample volume used for measurements could be increased. By applying larger volumes of sample, more α-synuclein

would possibly bind to the surface, possibly enhancing the differences between samples. Similarly, a pre-treatment of the samples to enrich disease specific synuclein could be introduced.

The evaluation of images could also be improved. In this study, over all fluorescence intensity of the images was the only dimension used in evaluation. The images, however, contain more information that could be used to differentiate between samples. The amount, size and intensity of objects can theoretically all be classified, provided an appropriated algorithm is found or created. (The potential for) Such a multidimensional analysis is not feasible in common immunosorbent assays in contrast, sFIDA has great potential to reveal even subtle differences in samples that show equal fluorescence intensities.

In theory it is also possible to use more than two labelled antibodies and measure additional channel accordingly. Since the disease specific aggregates like Lewy bodies and glial cytoplasmic inclusions often include other proteins such as tau or ubiquitin, colocalisation of antibodies against these proteins could help to increase the specificity of the sFIDA for disease related aggregates. It would also be possible to measure biomarkers not associated directly with the aggregates in the same assay.

The decreased signal intensity in samples taken from PD patients seems to correlate with lowered total α-synuclein content reported for CSF samples derived from PD and MSA patients (Mondello, 2014; Wang, 2012). Using an immunosorbent assay however, an increase in content of oligomeric α-synuclein aggregates has been observed in CSF from PD patients (Park et al. 2011, Tokuda et al. 2010). Similarly, samples with a higher signal in comparison to control have been reported for Amyloid-β oligomers in AD and for disease-associated aggregates of prion protein in sheep using sFIDA (Bannach et al. 2012, Wang-Dietrich et al. 2013).

A CSF sample taken post mortem from a patient with MSA showed a much higher signal than the control. Further studies must be concluded to determine whether this was coincidental or if there is a characteristic difference in α-synuclein content in relation to disease progression. To evaluate a possible correlation between aggregate content and disease progression, studies with samples taken at intervals over a longer timeframe should be performed and compared to post mortem levels of α-synuclein.

In conclusion, although α-synuclein aggregates can be detected in CSF, sFIDA needs to be further optimised for the differentiation between samples from patients with MSA and PD and healthy controls. The results for the PD samples are promising, but thorough investigation of a large amount of clinical samples representing different stages of both diseases needs to be performed. Variation

of the antibodies has a high chance of improving sensitivity and specificity, and there is a lot of potential in expanding the observed dimension in the evaluation.

5 Summary

Synucleinopathies are a group of neurodegenerative disorders all characterised by the aggregation of misfolded α-synuclein. The symptoms, caused by neuronal cell death, range from motor skill impairment and dementia to psychological deficiencies and sleep disorders. These symptoms, which usually first appear years after disease onset, are the basis for clinical diagnosis.

However, due to their late onset and a significant overlap of symptoms among synucleinopathies and also other neurodegenerative diseases, diagnosis is often complicated. Therefore, the search for a biomarker which can assist the diagnosis is of great importance to advance knowledge of the disease and reveal possible treatments.

α-synuclein is a potential candidate for such a biomarker. Its aggregated state is a common biochemical feature of synucleinopathies and growing evidence suggests that its level decreases in CSF with disease progression.

In this work, sFIDA was developed for the detection of α-synuclein exclusively in its aggregated state. First, the expression and purification of α-synuclein in high amounts and of high purity was established. Subsequently, different aggregation assays were compared and the biophysical properties of the aggregates were measured. CD spectroscopy, amyloid-specific ThT fluorescence and AFM imaging confirmed the formation of amyloid fibrils, which were used to establish sFIDA. Different conditions for storing the fibrils were tested and evaluated by analysing change in fibril content by absorption spectroscopy as well as change in fibril morphology by AFM. Antibodies to be used in sFIDA were fluorescently labelled. SPR measurements proved that labelling did not interfere with the ability of the antibodies to bind α-synuclein fibrils. Testing different combinations of antibodies for sFIDA revealed that the choice of the capture antibody is critical, as a dependence of signal strength on protein content of samples could only be achieved with antibody 211 as the capture. Variation in the choice of detection antibodies did not show a significant influence on measurements.

After the adaptation of sFIDA for α-synuclein was accomplished, measurements showed that it was selective for the detection of aggregates and not monomers with a sensitivity of at least 1 pg/mL. Detection of recombinant aggregates in CSF in a concentration dependent manner was also shown. Analysis of CSF samples from patients with MSA and PD showed that the assay must still be optimised, but variation of antibodies and improved evaluation can easily be implemented and show great potential to increase sensitivity and specificity of the assay.

6 Zusammenfassung

Synukleinopathien sind eine Gruppe von neurodegenerativen Krankheiten, die alle durch die Aggregation von fehlgefaltenem α-Synuklein charakterisiert werden. Die durch den Tod neuronaler Zellen ausgelösten Symptome umfassen Bewegungsstörungen, Demenz, psychologische Beschwerden und Schlafstörungen. Diese Symptome, die oft erst Jahre nach dem eigentlichen Einsetzen der Krankheit auftreten, bilden die Grundlage der klinischen Diagnose.

Aufgrund des späten Einsetzens der Symptome und den starken Überschneidungen der Symptome nicht nur innerhalb der Synukleinopathien selbst, sondern auch mit anderen neurodegenerativen Krankheiten, ist die Diagnose meist kompliziert. Deshalb ist die Suche nach einem Biomarker der die Diagnose unterstützt ausgesprochen wichtig um genauer Kenntnisse über den Verlauf der Krankheit und möglicher Therapien zu erhalten.

α-Synuklein ist ein Kandidat für einen solchen Biomarker. Seine aggregierte Form ist das verbindende biochemische Merkmal der Synukleinopathien und es gibt vermehrt Belege dafür dass sich der α-Synukleingehalt im Krankheitsverlauf senkt.

In dieser Arbeit wurde das sFIDA für die Detektion von α-Synukleinaggregaten entwickelt. Zuerst wurde die Aufreinigung von großen Mengen hochreinen α-Synukleins etabliert. Daraufhin wurden verschiedene Methoden zur Aggregation getestet und verglichen und anschließend die biophysikalischen Eigenschaften der Aggregate verglichen. Mittels CD-Spektroskopie, amyloid-spezifischer Fluoreszenz des Farbstoffs ThT und AFM wurde die Bildung amyloider Fibrillen bestätigt, welche im Anschluss zur Etablierung des sFIDA eingesetzt wurden. Unterschiedliche Lagerbedingungen der Fibrillen wurden getestet und anhand der Konzentrationsänderung und des Erscheinungsbildes der Fibrillen im AFM verglichen. Antikörper wurden zur Verwendung im sFIDA mit Fluoreszenzfarbstoffen markiert und SPR Messungen zeigten keine Beeinträchtigung der Bindung von Antikörpern an Fibrillen durch die Markierung. Das Austesten verschiedener Kombinationen von Antikörpern im sFIDA zeigte das eine Abhängigkeit des Signals von der Proteinmenge nur gegeben ist wenn Antikörper 211 als Capture eingesetzt wird, während die Kombination der Detektionsantikörper keinen großen Einfluss hat.

Nach der erfolgreichen Anpassung des sFIDA an die Messung von α-Synuklein wurde gezeigt, dass selektiv Aggregate und nicht Monomere gemessen wurden, mit einer Sensitivität von mindestens 1 pg/mL. Die gilt auch wenn die Aggregate in Liquor verdünnt werden.

Die Analyse von Liquorproben von MSA- und PD-Patienten zeigte, dass das Assay noch optimiert werden muss, aber ein Austausch der Antikörper und ein Ausbau der Auswertung sind leicht zu implementieren und besitzen viel Potential die Sensitivität und Spezifität des Assays zu verbessern.

7 List of Figures and Tables

7.1 Figures

Figure 1: α-synuclein primary structure 7
Figure 2: Negative stained TEM images of different fibril morphologies 8
Figure 3: Example of fibril identification by ThT fluorescence 9
Figure 4: Setup of sFIDA assay 12
Figure 5: Concept of the colocalisation process 33
Figure 6: Exemplary illustration of the cutoff 35
Figure 7: Western blot showing the induction of α-synuclein expression 37
Figure 8: SDS-PAGE of the purification process of α-synuclein, stained with Coomassie Brilliant Blue 38
Figure 9: Western blot of purified α-synuclein. 39
Figure 10: Ion exchange chromatography during α-synuclein purification 40
Figure 12: Chromatogram from purification of α-synuclein by SEC 41
Figure 13: CD spectra of α-synuclein fibril formation in MES buffer 42
Figure 14: CD spectra of fibril formation in Tris buffer 43
Figure 15: CD spectra of α-synuclein fibril formation in NaP_i/SDS buffer 43
Figure 16: Amyloid fibril formation of α-synuclein in different buffers followed by increased ThT fluorescence 44
Figure 17: α-synuclein fibrils formed in MES buffer measured by AFM 45
Figure 18: α-synuclein fibrils formed in Tris buffer measured by AFM 46
Figure 19: α-synuclein fibrils formed in NaP_i/SDS buffer measure by AFM 47
Figure 20: sFIDA shows correlation between signal strength and amount of aggregates matured and diluted in different buffers 48
Figure 21: sFIDA shows correlation between singal strenght and amount of fibrils matured in different buffers diluted in human CSF 49
Figure 22: α-synuclein fibril imaged by AFM before storage 51
Figure 23: α-synuclein fibril imaged by AFM after storage at 4 °C 51
Figure 24: α-synuclein fibrils imaged by AFM after storage at -80 °C 51
Figure 25: α-synuclein fibrils imaged by AFM after storage at -80 °C in lyophilised form 52
Figure 26: sFIDA of fibrils stored under different conditions shows slight loss of intensity depending on storage conditions 53
Figure 27: SPR measurements of labelled and unlabelled antibodies 55

Figure 28: Comparison of sFIDA signal from different antibody combinations 56
Figure 29: Influence of different capture antibodies on sFIDA 58
Figure 30: sFIDA is not impaired by CSF or monomeric α-synuclein 59
Figure 31: Influence of CSF and monomeric α-synuclein on sFIDA measured by TIRFM 60
Figure 32: sFIDA of MSA samples, colocalised 61
Figure 33: sFIDA of PD samples, colocalised 62

7.2 Tables

Table 1: Buffers and solutions 14
Table 2: Antibodies 15
Table 5: Composition of gels for SDS-PAGE 19
Table 6: Conditions of α-synuclein aggregation 20
Table 7: Parameters for CD – spectroscopy measurements 21
Table 8: Parameters for the measurement of ThT fluorescence 22
Table 9: Parameters of TIRFM channels 30
Table 10: Parameters of the settings for the 2D Job "Steffen 2D" 32
Table 11: Concentration of soluble α-synuclein depending on storage conditions 50
Table 12: Kinetic parameters of the binding of antibody 211 to α-synuclein fibrils 54

8 Literature

National Collaborating Centre for Chronic Conditions. Parkinson's disease: national clinical guideline for diagnosis and management in primary and secondary care. London: Royal College of Physicians, 2006.

ACCHIONE M, LEE YC, DESANTIS ME, LIPSCHULTZ CA, WLODAWER A, LI M, SHANMUGANATHAN A, WALTER RL, SMITH-GILL S AND BARCHI JJ, JR. 2012. Specific fluorine labeling of the HyHEL10 antibody affects antigen binding and dynamics. Biochemistry 51: 6017-6027.

AERTS MB, ESSELINK RA, ABDO WF, BLOEM BR AND VERBEEK MM. 2012. CSF alpha-synuclein does not differentiate between parkinsonian disorders. Neurobiology of aging 33: 430 e431-433.

ALIM MA ET AL. 2004. Demonstration of a role for alpha-synuclein as a functional microtubule-associated protein. Journal of Alzheimer's disease : JAD 6: 435-442; discussion 443-439.

BABA M, NAKAJO S, TU PH, TOMITA T, NAKAYA K, LEE VM, TROJANOWSKI JQ AND IWATSUBO T. 1998. Aggregation of alpha-synuclein in Lewy bodies of sporadic Parkinson's disease and dementia with Lewy bodies. The American journal of pathology 152: 879-884.

BANNACH O, BIRKMANN E, REINARTZ E, JAEGER KE, LANGEVELD JP, ROHWER RG, GREGORI L, TERRY LA, WILLBOLD D AND RIESNER D. 2012. Detection of prion protein particles in blood plasma of scrapie infected sheep. PloS one 7: e36620.

BARTELS T, CHOI JG AND SELKOE DJ. 2011. alpha-Synuclein occurs physiologically as a helically folded tetramer that resists aggregation. Nature 477: 107-110.

BHAK G, LEE JH, HAHN JS AND PAIK SR. 2009. Granular assembly of alpha-synuclein leading to the accelerated amyloid fibril formation with shear stress. PloS one 4: e4177.

BIANCALANA M AND KOIDE S. 2010. Molecular mechanism of Thioflavin-T binding to amyloid fibrils. Biochimica et biophysica acta 1804: 1405-1412.

BIRKMANN E, HENKE F, WEINMANN N, DUMPITAK C, GROSCHUP M, FUNKE A, WILLBOLD D AND RIESNER D. 2007. Counting of single prion particles bound to a capture-antibody surface (surface-FIDA). Veterinary microbiology 123: 294-304.

BIRKMAYER W AND HORNYKIEWICZ O. 1998. The effect of l-3,4-dihydroxyphenylalanine (=DOPA) on akinesia in parkinsonism. Parkinsonism & related disorders 4: 59-60.

BOUSSET L ET AL. 2013. Structural and functional characterization of two alpha-synuclein strains. Nature communications 4: 2575.

BURN DJ AND JAROS E. 2001. Multiple system atrophy: cellular and molecular pathology. Molecular pathology : MP 54: 419-426.

CABIN DE ET AL. 2002. Synaptic vesicle depletion correlates with attenuated synaptic responses to prolonged repetitive stimulation in mice lacking alpha-synuclein. The Journal of neuroscience : the official journal of the Society for Neuroscience 22: 8797-8807.

CHANDRA S, GALLARDO G, FERNANDEZ-CHACON R, SCHLUTER OM AND SUDHOF TC. 2005. Alpha-synuclein cooperates with CSPalpha in preventing neurodegeneration. Cell 123: 383-396.

CHEN J, MILLS JD, HALLIDAY GM AND JANITZ M. 2014. The role of transcriptional control in multiple system atrophy. Neurobiology of aging.

COLLINS SR, DOUGLASS A, VALE RD AND WEISSMAN JS. 2004. Mechanism of prion propagation: amyloid growth occurs by monomer addition. PLoS biology 2: e321.

CONWAY KA, LEE SJ, ROCHET JC, DING TT, HARPER JD, WILLIAMSON RE AND LANSBURY PT, JR. 2000a. Accelerated oligomerization by Parkinson's disease linked alpha-synuclein mutants. Annals of the New York Academy of Sciences 920: 42-45.

CONWAY KA, LEE SJ, ROCHET JC, DING TT, WILLIAMSON RE AND LANSBURY PT, JR. 2000b. Acceleration of oligomerization, not fibrillization, is a shared property of both alpha-synuclein mutations linked to early-onset Parkinson's disease: implications for pathogenesis and therapy. Proceedings of the National Academy of Sciences of the United States of America 97: 571-576.

COOKSON MR, XIROMERISIOU G AND SINGLETON A. 2005. How genetics research in Parkinson's disease is enhancing understanding of the common idiopathic forms of the disease. Current opinion in neurology 18: 706-711.

DANZER KM, HAASEN D, KAROW AR, MOUSSAUD S, HABECK M, GIESE A, KRETZSCHMAR H, HENGERER B AND KOSTKA M. 2007. Different species of alpha-synuclein oligomers induce calcium influx and seeding. The Journal of neuroscience : the official journal of the Society for Neuroscience 27: 9220-9232.

DE LAU LM AND BRETELER MM. 2006. Epidemiology of Parkinson's disease. The Lancet Neurology 5: 525-535.

DONAGHY PC AND MCKEITH IG. 2014. The clinical characteristics of dementia with Lewy bodies and a consideration of prodromal diagnosis. Alzheimer's research & therapy 6: 46.

EL-AGNAF OM, SALEM SA, PALEOLOGOU KE, CURRAN MD, GIBSON MJ, COURT JA, SCHLOSSMACHER MG AND ALLSOP D. 2006. Detection of oligomeric forms of alpha-synuclein protein in human plasma as a potential biomarker for Parkinson's disease. FASEB journal : official publication of the Federation of American Societies for Experimental Biology 20: 419-425.

ESLER WP, STIMSON ER, JENNINGS JM, VINTERS HV, GHILARDI JR, LEE JP, MANTYH PW AND MAGGIO JE. 2000. Alzheimer's disease amyloid propagation by a template-dependent dock-lock mechanism. Biochemistry 39: 6288-6295.

FORTIN DL, TROYER MD, NAKAMURA K, KUBO S, ANTHONY MD AND EDWARDS RH. 2004. Lipid rafts mediate the synaptic localization of alpha-synuclein. The Journal of neuroscience : the official journal of the Society for Neuroscience 24: 6715-6723.

GIASSON BI, MURRAY IV, TROJANOWSKI JQ AND LEE VM. 2001. A hydrophobic stretch of 12 amino acid residues in the middle of alpha-synuclein is essential for filament assembly. The Journal of biological chemistry 276: 2380-2386.

GIEHM L, LORENZEN N AND OTZEN DE. 2011. Assays for alpha-synuclein aggregation. Methods 53: 295-305.

GIEHM L, OLIVEIRA CL, CHRISTIANSEN G, PEDERSEN JS AND OTZEN DE. 2010. SDS-induced fibrillation of alpha-synuclein: an alternative fibrillation pathway. Journal of molecular biology 401: 115-133.

GILMAN S ET AL. 1999. Consensus statement on the diagnosis of multiple system atrophy. Journal of the neurological sciences 163: 94-98.

GILMAN S ET AL. 2008. Second consensus statement on the diagnosis of multiple system atrophy. Neurology 71: 670-676.

HASHIMOTO M, KAWAHARA K, BAR-ON P, ROCKENSTEIN E, CREWS L AND MASLIAH E. 2004. The Role of alpha-synuclein assembly and metabolism in the pathogenesis of Lewy body disease. Journal of molecular neuroscience : MN 24: 343-352.

HEISE H, HOYER W, BECKER S, ANDRONESI OC, RIEDEL D AND BALDUS M. 2005. Molecular-level secondary structure, polymorphism, and dynamics of full-length alpha-synuclein fibrils studied by solid-state NMR. Proceedings of the National Academy of Sciences of the United States of America 102: 15871-15876.

HORVATH I ET AL. 2012. Mechanisms of protein oligomerization: inhibitor of functional amyloids templates alpha-synuclein fibrillation. Journal of the American Chemical Society 134: 3439-3444.

HOYER W, ANTONY T, CHERNY D, HEIM G, JOVIN TM AND SUBRAMANIAM V. 2002. Dependence of alpha-synuclein aggregate morphology on solution conditions. Journal of molecular biology 322: 383-393.

HOYER W, CHERNY D, SUBRAMANIAM V AND JOVIN TM. 2004. Impact of the acidic C-terminal region comprising amino acids 109-140 on alpha-synuclein aggregation in vitro. Biochemistry 43: 16233-16242.

HSU LJ, SAGARA Y, ARROYO A, ROCKENSTEIN E, SISK A, MALLORY M, WONG J, TAKENOUCHI T, HASHIMOTO M AND MASLIAH E. 2000. alpha-synuclein promotes mitochondrial deficit and oxidative stress. The American journal of pathology 157: 401-410.

IWAI A, MASLIAH E, YOSHIMOTO M, GE N, FLANAGAN L, DE SILVA HA, KITTEL A AND SAITOH T. 1995. The precursor protein of non-A beta component of Alzheimer's disease amyloid is a presynaptic protein of the central nervous system. Neuron 14: 467-475.

JAKES R, SPILLANTINI MG AND GOEDERT M. 1994. Identification of two distinct synucleins from human brain. FEBS letters 345: 27-32.

JANISSEN R, OBERBARNSCHEIDT L AND OESTERHELT F. 2009. Optimized straight forward procedure for covalent surface immobilization of different biomolecules for single molecule applications. Colloids and surfaces B, Biointerfaces 71: 200-207.

JANKOVIC J. 2008. Parkinson's disease: clinical features and diagnosis. Journal of neurology, neurosurgery, and psychiatry 79: 368-376.

JIMENEZ-JIMENEZ FJ, ALONSO-NAVARRO H, GARCIA-MARTIN E AND AGUNDEZ JA. 2014. Cerebrospinal fluid biochemical studies in patients with Parkinson's disease: toward a potential search for biomarkers for this disease. Frontiers in cellular neuroscience 8: 369.

JO E, DARABIE AA, HAN K, TANDON A, FRASER PE AND MCLAURIN J. 2004. alpha-Synuclein-synaptosomal membrane interactions: implications for fibrillogenesis. European journal of biochemistry / FEBS 271: 3180-3189.

KAHLE PJ ET AL. 2001. Selective insolubility of alpha-synuclein in human Lewy body diseases is recapitulated in a transgenic mouse model. The American journal of pathology 159: 2215-2225.

KAYED R ET AL. 2010. Conformation dependent monoclonal antibodies distinguish different replicating strains or conformers of prefibrillar Abeta oligomers. Molecular neurodegeneration 5: 57.

KAYED R ET AL. 2007. Fibril specific, conformation dependent antibodies recognize a generic epitope common to amyloid fibrils and fibrillar oligomers that is absent in prefibrillar oligomers. Molecular neurodegeneration 2: 18.

KOTZBAUER PT, TROJANOWSK JQ AND LEE VM. 2001. Lewy body pathology in Alzheimer's disease. Journal of molecular neuroscience : MN 17: 225-232.

LASHUEL HA, OVERK CR, OUESLATI A AND MASLIAH E. 2013. The many faces of alpha-synuclein: from structure and toxicity to therapeutic target. Nature reviews Neuroscience 14: 38-48.

LI C, LUTZ EA, SLADE KM, RUF RA, WANG GF AND PIELAK GJ. 2009. 19F NMR studies of alpha-synuclein conformation and fibrillation. Biochemistry 48: 8578-8584.

LIU S, NINAN I, ANTONOVA I, BATTAGLIA F, TRINCHESE F, NARASANNA A, KOLODILOV N, DAUER W, HAWKINS RD AND ARANCIO O. 2004. alpha-Synuclein produces a long-lasting increase in neurotransmitter release. The EMBO journal 23: 4506-4516.

MAROTEAUX L, CAMPANELLI JT AND SCHELLER RH. 1988. Synuclein: a neuron-specific protein localized to the nucleus and presynaptic nerve terminal. The Journal of neuroscience : the official journal of the Society for Neuroscience 8: 2804-2815.

MARTI MJ, TOLOSA E AND CAMPDELACREU J. 2003. Clinical overview of the synucleinopathies. Movement disorders : official journal of the Movement Disorder Society 18 Suppl 6: S21-27.

MCCANN H, STEVENS CH, CARTWRIGHT H AND HALLIDAY GM. 2014. alpha-Synucleinopathy phenotypes. Parkinsonism & related disorders 20 Suppl 1: S62-67.

MOLLENHAUER B, EL-AGNAF OM, MARCUS K, TRENKWALDER C AND SCHLOSSMACHER MG. 2010. Quantification of alpha-synuclein in cerebrospinal fluid as a biomarker candidate: review of the literature and considerations for future studies. Biomarkers in medicine 4: 683-699.

MOLLENHAUER B, LOCASCIO JJ, SCHULZ-SCHAEFFER W, SIXEL-DÖRING F, TRENKWALDER C AND SCHLOSSMACHER MG. 2011. α-Synuclein and tau concentrations in cerebrospinal fluid of patients presenting with parkinsonism: a cohort study. The Lancet Neurology 10: 230-240.

MONDELLO S, CONSTANTINESCU R, ZETTERBERG H, ANDREASSON U, HOLMBERG B AND JEROMIN A. 2014. CSF alpha-synuclein and UCH-L1 levels in Parkinson's disease and atypical parkinsonian disorders. Parkinsonism & related disorders 20: 382-387.

MURPHY DD, RUETER SM, TROJANOWSKI JQ AND LEE VM. 2000. Synucleins are developmentally expressed, and alpha-synuclein regulates the size of the presynaptic vesicular pool in primary hippocampal neurons. The Journal of neuroscience : the official journal of the Society for Neuroscience 20: 3214-3220.

NELSON R, SAWAYA MR, BALBIRNIE M, MADSEN AO, RIEKEL C, GROTHE R AND EISENBERG D. 2005. Structure of the cross-beta spine of amyloid-like fibrils. Nature 435: 773-778.

PAPP MI, KAHN JE AND LANTOS PL. 1989. Glial cytoplasmic inclusions in the CNS of patients with multiple system atrophy (striatonigral degeneration, olivopontocerebellar atrophy and Shy-Drager syndrome). Journal of the neurological sciences 94: 79-100.

PARK MJ, CHEON SM, BAE HR, KIM SH AND KIM JW. 2011. Elevated levels of alpha-synuclein oligomer in the cerebrospinal fluid of drug-naive patients with Parkinson's disease. Journal of clinical neurology 7: 215-222.

PARNETTI L ET AL. 2014a. Cerebrospinal fluid lysosomal enzymes and alpha-synuclein in Parkinson's disease. Movement disorders : official journal of the Movement Disorder Society 29: 1019-1027.

PARNETTI L ET AL. 2014b. Differential role of CSF alpha-synuclein species, tau, and Abeta42 in Parkinson's Disease. Frontiers in aging neuroscience 6: 53.

ROCHET JC, CONWAY KA AND LANSBURY PT, JR. 2000. Inhibition of fibrillization and accumulation of prefibrillar oligomers in mixtures of human and mouse alpha-synuclein. Biochemistry 39: 10619-10626.

SAMII A, NUTT JG AND RANSOM BR. 2004. Parkinson's disease. Lancet 363: 1783-1793.

SAWAYA MR ET AL. 2007. Atomic structures of amyloid cross-beta spines reveal varied steric zippers. Nature 447: 453-457.

SCOTT DA, TABAREAN I, TANG Y, CARTIER A, MASLIAH E AND ROY S. 2010. A pathologic cascade leading to synaptic dysfunction in alpha-synuclein-induced neurodegeneration. The Journal of neuroscience : the official journal of the Society for Neuroscience 30: 8083-8095.

SERPELL LC, BERRIMAN J, JAKES R, GOEDERT M AND CROWTHER RA. 2000. Fiber diffraction of synthetic alpha-synuclein filaments shows amyloid-like cross-beta conformation. Proceedings of the National Academy of Sciences of the United States of America 97: 4897-4902.

SIDHU A, WERSINGER C AND VERNIER P. 2004. Does alpha-synuclein modulate dopaminergic synaptic content and tone at the synapse? FASEB journal : official publication of the Federation of American Societies for Experimental Biology 18: 637-647.

SPILLANTINI MG, CROWTHER RA, JAKES R, CAIRNS NJ, LANTOS PL AND GOEDERT M. 1998. Filamentous alpha-synuclein inclusions link multiple system atrophy with Parkinson's disease and dementia with Lewy bodies. Neuroscience letters 251: 205-208.

SPILLANTINI MG AND GOEDERT M. 2000. The alpha-synucleinopathies: Parkinson's disease, dementia with Lewy bodies, and multiple system atrophy. Annals of the New York Academy of Sciences 920: 16-27.

TASCHENBERGER G, GARRIDO M, TERESHCHENKO Y, BAHR M, ZWECKSTETTER M AND KUGLER S. 2012. Aggregation of alphaSynuclein promotes progressive in vivo neurotoxicity in adult rat dopaminergic neurons. Acta neuropathologica 123: 671-683.

TATENO F, SAKAKIBARA R, KAWAI T, KISHI M AND MURANO T. 2012. Alpha-synuclein in the cerebrospinal fluid differentiates synucleinopathies (Parkinson Disease, dementia with Lewy bodies, multiple system atrophy) from Alzheimer disease. Alzheimer disease and associated disorders 26: 213-216.

TOKUDA T, QURESHI MM, ARDAH MT, VARGHESE S, SHEHAB SA, KASAI T, ISHIGAMI N, TAMAOKA A, NAKAGAWA M AND EL-AGNAF OM. 2010. Detection of elevated levels of alpha-synuclein oligomers in CSF from patients with Parkinson disease. Neurology 75: 1766-1772.

TOTTERDELL S AND MEREDITH GE. 2005. Localization of alpha-synuclein to identified fibers and synapses in the normal mouse brain. Neuroscience 135: 907-913.

TROJANOWSKI JQ AND GROWDON JH. 1998. A new consensus report on biomarkers for the early antemortem diagnosis of Alzheimer disease: current status, relevance to drug discovery, and recommendations for future research. Journal of neuropathology and experimental neurology 57: 643-644.

TSIGELNY IF ET AL. 2008. Mechanisms of hybrid oligomer formation in the pathogenesis of combined Alzheimer's and Parkinson's diseases. PloS one 3: e3135.

UCHIKADO H, LIN WL, DELUCIA MW AND DICKSON DW. 2006. Alzheimer disease with amygdala Lewy bodies: a distinct form of alpha-synucleinopathy. Journal of neuropathology and experimental neurology 65: 685-697.

UEDA K, FUKUSHIMA H, MASLIAH E, XIA Y, IWAI A, YOSHIMOTO M, OTERO DA, KONDO J, IHARA Y AND SAITOH T. 1993. Molecular cloning of cDNA encoding an unrecognized component of amyloid in Alzheimer disease. Proceedings of the National Academy of Sciences of the United States of America 90: 11282-11286.

UVERSKY VN. 2007. Neuropathology, biochemistry, and biophysics of alpha-synuclein aggregation. Journal of neurochemistry 103: 17-37.

VILAR M, CHOU HT, LUHRS T, MAJI SK, RIEK-LOHER D, VEREL R, MANNING G, STAHLBERG H AND RIEK R. 2008. The fold of alpha-synuclein fibrils. Proceedings of the National Academy of Sciences of the United States of America 105: 8637-8642.

WAKABAYASHI K, TANJI K, MORI F AND TAKAHASHI H. 2007. The Lewy body in Parkinson's disease: molecules implicated in the formation and degradation of alpha-synuclein aggregates. Neuropathology : official journal of the Japanese Society of Neuropathology 27: 494-506.

WANG-DIETRICH L, FUNKE SA, KUHBACH K, WANG K, BESMEHN A, WILLBOLD S, CINAR Y, BANNACH O, BIRKMANN E AND WILLBOLD D. 2013. The amyloid-beta oligomer count in cerebrospinal fluid is a biomarker for Alzheimer's disease. Journal of Alzheimer's disease : JAD 34: 985-994.

WANG Y ET AL. 2012. Phosphorylated alpha-synuclein in Parkinson's disease. Science translational medicine 4: 121ra120.

WARNER TT AND SCHAPIRA AH. 2003. Genetic and environmental factors in the cause of Parkinson's disease. Annals of neurology 53 Suppl 3: S16-23; discussion S23-15.

WEINREB PH, ZHEN W, POON AW, CONWAY KA AND LANSBURY PT, JR. 1996. NACP, a protein implicated in Alzheimer's disease and learning, is natively unfolded. Biochemistry 35: 13709-13715.

WINNER B ET AL. 2011. In vivo demonstration that alpha-synuclein oligomers are toxic. Proceedings of the National Academy of Sciences of the United States of America 108: 4194-4199.

WOOD SJ, WYPYCH J, STEAVENSON S, LOUIS JC, CITRON M AND BIERE AL. 1999. alpha-synuclein fibrillogenesis is nucleation-dependent. Implications for the pathogenesis of Parkinson's disease. The Journal of biological chemistry 274: 19509-19512.

GOLDMAN SM AND TANNER C. 2007 Etiology of Parkinson's disease. In: Jankovic J, Tolosa E (eds). Parkinson's disease and movement disorders. 3rd ed. Baltimore: Williams and Wilkins:1998:133-158.

Eidesstattliche Erklärung

Hiermit erkläre ich an Eides statt, dass ich diese Arbeit selbständig verfasst und keine anderen als die angegebenen Hilfsmittel und Quellen verwendet, sowie alle Quellen kenntlich gemacht habe.

Düsseldorf, den

(Steffen Hübinger)

Danksagung

Hiermit möchte ich all jenen danken, die mich während dieser Arbeit begleitet und unterstützt haben.

An erster Stelle möchte ich Prof. Dr. Dieter Willbold dafür danken, dass er mir die Möglichkeit gegeben hat diese Arbeit am Institut für Physikalische Biologie anzufertigen. Prof. Dr. Alfons Schnitzler danke ich dafür, dass er sich als Betreuer im Rahmen der iGRASP$_{seed}$ Graduiertenschule und als Zweitgutachter dieser Arbeit zur Verfügung gestellt hat.

Mein Dank gilt auch der gesamten Arbeitsgruppe Birkmann für die fortwährende Unterstützung, für kritische Diskussionen und aufbauende Worte. Dr. Eva Birkmann und Dr. Oliver Bannach danke ich für die Betreuung. Elke Reinartz danke ich für ihre stete Hilfsbereitschaft und Unterstützung bei allen kleinen und großen Fragen und Aufgaben des wissenschaftlichen Alltags.

Tommy, Sabine, Lars, Jendrik, Ilka, Barbara und Michael danke ich für viele ernste und lustige, sinnstiftende und nichtssagende Gespräche im Büro und im Labor, am Herd und am Eisen, bei Kaffee, Tee oder Hopfensaft. Daran werde ich immer gerne zurückdenken!

Bernd danke ich für die Hilfe bei den tausend kleinen Alltagsdingen ebenso wie für die ausführlichen Übungen im Rätseln und Querdenken.

Ein besonderer Dank geht auch an Heidi für ihre stete Hilfsbereitschaft und dafür, dass sie stets Geduld für die wissenschaftlichen Freigeister aufbringen konnte.

Wolfgang danke ich für die Hilfe und stete Diskussionsbereitschaft.

Natürlich danke ich auch meiner Familie, die mich auch in dieser Zeit unterstützt und aufgebaut hat.

Ewa, Dir danke ich ganz besonders. Ohne Deine Unterstützung im fachlichen wie im privaten, ohne deinen Einsatz und deine Hilfsbereitschaft wäre diese Arbeit nicht möglich gewesen!